Title

Electron-Affinity Time-Dependent Density Functional Theory: Formalism and Applications to Core-Excited States

Journal

The Journal of Physical Chemistry Letters, 13(41)

ISSN

1948-7185

Authors

Carter-Fenk, Kevin

Cunha, Leonardo A

Arias-Martinez, Juan E

et al.

Publication Date

2022-10-20

DOI

10.1021/acs.jpclett.2c02564

Electron-Affinity Time-Dependent Density Functional Theory: Formalism and Applications to Core-Excited States

Kevin Carter-Fenk,* Leonardo A. Cunha,* Juan E. Arias-Martinez,* and Martin Head-Gordon*
Kenneth S. Pitzer Center for Theoretical Chemistry,
Department of Chemistry, University of California, Berkeley, CA 94720, USA
Chemical Sciences Division, Lawrence Berkeley National Laboratory, Berkeley, CA 94720, USA
(Dated: September 21, 2022)

The particle-hole interaction problem is longstanding within time-dependent density functional theory (TDDFT) and leads to extreme errors in the prediction of K-edge X-ray absorption spectra (XAS). We derive a linear-response formalism that uses optimized orbitals of the n–1-electron system as reference, building orbital relaxation and a proper hole into the initial density. Our approach is an exact generalization of the static-exchange approximation that ameliorates particle-hole interaction error associated with the adiabatic approximation and reduces errors in TDDFT XAS by orders of magnitude. With a statistical performance of just 0.5 eV root-mean-square error and the same computational scaling as TDDFT under the core-valence separation approximation, we anticipate that this approach will be of great utility in XAS calculations of large systems.

TOC Graphic

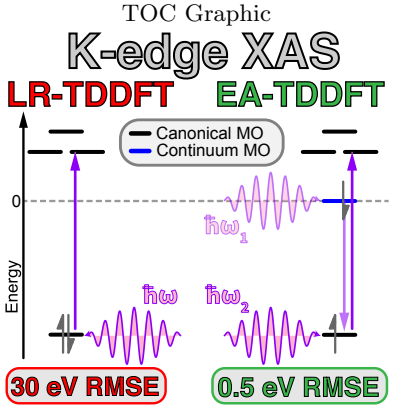

Recent advancements in synchrotron and ultrafast tabletop X-ray light-sources mark the dawn of an X-ray technology renaissance. With exceptional element-specificity, X-ray spectroscopy has found use in probing liquid-to-metal phase transitions of ammonia,[1] tracking charge-separation dynamics in dye-sensitized solar cells and organic light-harvesting systems,[2,3] and has revealed quantum nuclear dynamics near conical intersections.[4] Modern X-ray absorption spectroscopy (XAS) is capable of energy resolution on the order of 0.2–0.9 eV,[5] which is well below the error statistics of most modern theoretical methods that are routinely used to model XAS.

Linear-response time-dependent density functional theory (TDDFT) is by far the most commonly used method for computing excitation energies due its accuracy and efficiency.[6–11] While formally exact for excitation energies, TDDFT in practice is approximate due to inexact ground state functionals and the ubiquitous adiabatic approximation (henceforth assumed).[6,12,13] Although TDDFT achieves statistical accuracy of ∼0.2–0.3 eV for valence excitations,[14] errors increase dramatically for core excitations, often requiring empirical shifts on the order of 10–100 eV to realign the calculated spectra with experiment.[15–18] While range-separated hybrid functionals perform better in this regard,[19,20] specialized short-range corrected (SRC) functionals that feature a large amount of short-range Hartree-Fock (HF) exchange to correct for differential self-interaction error in the core have also been used instead of empirical shifting, albeit to the disregard of broader thermochemical properties.[21–28] Apart from pure TDDFT, semi-empirical extensions of configuration interaction that employ Kohn-Sham orbitals have been applied with some success to core-excitations.[29–31] In some cases, particularly in periodic systems, TDDFT and configuration-interaction methods are sidestepped in favor of cruder approaches like the Slater transition or transition potential methods.[32–40] Despite the myriad ways in which XAS can be calculated, in this work our focal point is linear-response TDDFT.

One source of error in predicting core-excitations using linear-response theory is the large orbital relaxation effect that follows from the displacement of charge out of a core orbital.[41,42] This can be addressed on a state-by-state basis using orbital-optimized density functional theory (OO-DFT), which explicitly relaxes the orbitals of excited-state configurations.[43] While OO-DFT routinely achieves a statistical accuracy of ∼0.3 eV for core-excitations,[44,45] state-by-state optimization is far less efficient than full-spectrum methods like TDDFT.

OO-DFT also requires some *a priori* knowledge of the system, complicating the selection of the "correct" set of bespoke determinants in systems with a high density of states.

Orbital relaxation error is related to the fundamentally incorrect particle-hole interaction in TDDFT descriptions of core-excited states.[46–48] This is the major source of error in TDDFT; emerging from the fact that the virtual orbitals in DFT are optimized in the n-electron potential, causing incomplete cancellation of the interaction of the excited electron with itself in the (previously occupied) core orbital. For example, consider the pure particle-hole interaction that results from exciting an electron between two molecular orbitals (MOs) that have zero overlap. For global hybrid functionals, the only nonzero elements of the orbital Hessians belong to the **A** matrix,

$$A_{ia,jb} = (\varepsilon_a - \varepsilon_i)\delta_{ij}\delta_{ab} - C_{\mathrm{HF}}(ij|ab) \tag{1}$$

where C_{HF} is the coefficient of HF exchange. The Coulomb interaction $(aa|ii)$ is included in the orbital energy difference and only in the case of exact exchange ($C_{\mathrm{HF}} = 1$) is this interaction properly cancelled by the third term in Eq. 1, leading to particle-hole attraction. Therefore with approximate density functionals, the excited electron "feels" a residual Coulomb potential from its unexcited image rather than a proper particle-hole attraction, causing core-excitation energies to be dramatically underestimated in approximate TDDFT.

In this letter, we introduce a linear-response TDDFT formalism that effectively models particle creation in the virtual space from an n–1-electron reference density. This way, orbital relaxation and information about the core hole are built directly into the reference density, completely eliminating electron-hole self-interaction error (eh-SIE) by construction. Our method generalizes the static-exchange approximation (STEX) into a density functional theory (DFT) framework.

Such generalizations have recently been proposed based purely on error cancellation between restricted open-shell Kohn-Sham (ROKS) theory and STEX,[49] but this work aims at a fully derivable formalism. Herein we demonstrate multifaceted benefits of an exact approach, including better overall performance, and a recovery of the Jacob's Ladder concept in DFT. While TDDFT is the workhorse of excited-state calculations in quantum chemistry, we further note that the concept of adding electrons to an n–1-electron reference determinant has been employed within Green's function based GW methods[50,51] and within algebraic diagrammatic construction approaches[52,53] to account for orbital relaxation and (in the case of GW theory) for a more appropriate description of particle-hole interactions. In principle, our proposed approach recovers the same poles as the single-particle Green's function in the electron addition domain. However, unlike GW approaches that scale roughly as $\mathcal{O}(N^4)$ with a nontrivial prefactor (where N is the number of basis functions),[54] our proposed approach has the same scaling as STEX ($\mathcal{O}[V^3]$, where V is the number of unoccupied MOs), making this a far more appealing method for large systems.

The STEX formalism has been used to improve upon core-excitation energies offered by configuration interaction with single excitations (CIS)[47,55,56] for a number of years.[57,58] In brief, STEX involves optimizing the MOs of the n–1-electron (core-ionized) system, followed by an electron-affinity CIS (EA-CIS) calculation to reattach the missing electron to the virtual orbitals, thereby yielding a partially orbital-optimized core-excitation spectrum that accounts for the strong polarization effect from creating a core hole. For a closed-shell reference, the EA-CIS equations for singlet states take the form,

$$A_{ia,ib} = E_{\mathrm{HF}}^{(n-1)}\delta_{ab} + F_{ab}^{(n-1)} + (ia|ib) \ , \tag{2}$$

where i is the core hole MO, $E_{\mathrm{HF}}^{(n-1)}$ is the core-ionized reference energy, $F_{ab}^{(n-1)}$ are elements of the virtual-virtual block of the core-ionized Fock matrix, and $(ia|ib)$ is an exchange integral in the standard Mulliken notation. Diagonalizing **A** results in states that are orthogonal to the core-ionized reference determinant, but are not orthogonal to the original n-electron ground state. The final step of the STEX procedure involves constructing nonorthogonal configuration interaction (NOCI) elements to project the n-electron ground state out of the Hamiltonian prior to diagonalizing, ensuring that all excited states are strictly orthogonal to the initial n-electron ground state determinant.[59–61] Herein, we will show that the nonorthogonality of the excited states to the ground state can be safely ignored when calculating K-edge XAS with almost no impact on the predicted excitation energies or transition properties, thus paving the way for a TDDFT formalism where the ambiguity of DFT-based NOCI elements once hindered such developments.

In order to generalize STEX to a TDDFT framework, we will use continuum MOs as a derivation tool. For our purposes, continuum MOs are fictitious, ultra-diffuse orbitals that do not interact with other MOs in the system and have zero energy. They offer utility in derivations of particle-nonconserving processes by recasting particle creation/annihilation into the language of particle-conserving excitations.[62]Throughout this work, we reserve the labels $\{j, k, l, \dots\}$ to denote occupied MOs, $\{a, b, c, \dots\}$ for the virtual MOs, and $\{p, q, r, \dots\}$ refer to general orbitals. Specific notation is reserved for the continuum MO, designated as x, and the core-hole MO, i.

To ameliorate orbital relaxation error, we begin with the self-consistently optimized MOs for the core-ionized system. We are interested in a protocol that uses particle-conserving excitations that emulate the action of the particle creation operator on our core-ionized reference,

$$|\Psi_i^a\rangle = \hat{a}_a^\dagger|\Psi_0\rangle \ , \tag{3}$$

where $|\Psi_0\rangle$ is the core-ionized reference determinant, and $\hat{a}_a^\dagger$ is the creation operator. One possibility that retains

correlations between single excitations in the response theory that follows is to consider two successive excitations $x \rightarrow i$ and $i \rightarrow a$ out of a modified core-ionized reference determinant that includes a single continuum MO. Conceptually, this can be likened to excited-state absorption where the n-electron state with the core-hole MO reoccupied acts as the intermediate state. In operator form it can be readily shown that,

$$|\Psi_i^a\rangle = \hat{a}_a^\dagger \hat{a}_i \hat{a}_i^\dagger \hat{a}_x |\Psi_0 \chi_x\rangle = \hat{a}_a^\dagger \hat{a}_i \hat{a}_i^\dagger |\Psi_0\rangle = \hat{a}_a^\dagger |\Psi_0\rangle \ , \quad (4)$$

where $|\Psi_0 \chi_x\rangle$ is the modified core-ionized reference, containing the noninteracting spin-orbital χ_x. This exercise reveals that the successive particle-conserving excitations $x \rightarrow i$ and $i \rightarrow a$ indeed reduce to particle creation in orbital a of the *unmodified* core-ionized reference determinant, which itself can be viewed as the tensor product of the core-ionized reference with the vacuum level in the space of continuum orbitals.

In order to capture this process in the language of density matrices, such that our protocol is amenable to DFT, we consider two successive linear responses. The first response generates the n-electron density from the n–1-electron reference by exciting an electron from a continuum MO into the core hole, and the second response yields eh-SIE-corrected excitations of this (newly added) core electron into the virtual space. Throughout this derivation, we follow the density matrix formalism starting from the Liouville-von Neumann equation,[9,47]

$$i\frac{\partial \mathbf{P}(t)}{\partial t} = [\mathbf{F}(t), \mathbf{P}(t)] \ . \quad (5)$$

The first response is obtained by restricting the excitation space to the (occupied) continuum MO and the (unoccupied) core-hole to yield,

$$\begin{aligned} A_{xi,xi} &= F_{ii}^{(n-1)} \\ B_{xi,xi} &= 0 \end{aligned} \quad (6)$$

Because the continuum MO does not interact with the rest of the system, all two-electron integrals involving the continuum MO vanish to give an expression that corresponds to the negative electron affinity in the limit of the exact functional.[63] Importantly, no orbital rotations are encoded in this response, meaning that the (idempotent) n-electron density can be exactly constructed with the n–1-electron MOs to linear order.

At some time $t' > t$, we apply a second time-varying electric field to the perturbed n-electron system. By regenerating the n-electron system, we have reintroduced eh-SIE, so we now seek to separate the response due to the presence of the core electron from the remainder of the response to the applied field. Assuming that the n-electron density is not too far from a stationary point, we may write the perturbed density and corresponding Fock matrices as,

$$\begin{aligned} \mathbf{P}(t') &= \mathbf{P}_0^{(n)} + \delta\mathbf{P}_{\mathrm{CO}}(t') + \delta\mathbf{P}_{\mathrm{EF}}(t') \\ \mathbf{F}(t') &= \mathbf{F}_0^{(n)} + \delta\mathbf{F}_{\mathrm{CO}}(t') + \delta\mathbf{F}_{\mathrm{EF}}(t') \end{aligned} \quad (7)$$

where $\mathbf{P}_0^{(n)}$ is the static part of the n-electron density, $\delta\mathbf{P}_{\mathrm{CO}}(t')$ represents the component of the response due to the (now occupied) core MO and $\delta\mathbf{P}_{\mathrm{EF}}(t')$ indicates the response of the n-electron system to the second electric field. Substituting Eq. 7 into Eq. 5 and keeping the terms that are linear with respect to the perturbing field leads to,

$$\begin{aligned} i\frac{\partial \delta\mathbf{P}_{\mathrm{CO}}(t')}{\partial t'} + i\frac{\partial \delta\mathbf{P}_{\mathrm{EF}}(t')}{\partial t'} &= [\mathbf{F}_0^{(n)}, \delta\mathbf{P}_{\mathrm{CO}}(t')] \\ + [\delta\mathbf{F}_{\mathrm{CO}}(t'), \mathbf{P}_0^{(n)}] + [\mathbf{F}_0^{(n)}, \delta\mathbf{P}_{\mathrm{EF}}(t')] &+ [\delta\mathbf{F}_{\mathrm{EF}}(t'), \mathbf{P}_0^{(n)}] \end{aligned} \ , \quad (8)$$

which is simply the sum of two linear responses. Notably, this formalism has been used to subtract nonstationary oscillations out of real-time TDDFT simulations of excited-state absorption (including application to transient XAS), and we have adopted similar notation throughout.[64–68]

We use the fact that the above responses are uncoupled to correct the n-electron response by subtracting the components that emerge due to the occupied core orbital *via* the difference Fock matrix,

$$\begin{aligned} F_{pq}^{\mathrm{CO}} &= F_{pq}^{(n)} - F_{pq}^{(n-1)} \\ &= (ii|pq) - C_{\mathrm{HF}}(ip|iq) \\ &\quad + (1 - C_{\mathrm{HF}})(p|V_{\mathrm{xc}}^{(n)} - V_{\mathrm{xc}}^{(n-1)}|q) \end{aligned} \quad (9)$$

and its corresponding density (all n-electron quantities are constructed using the n–1-electron MOs). This form of the Fock matrix incorporates all zeroth-order couplings between n- and n–1-electron potentials without approximation, and the corresponding difference density is idempotent with one electron in core MO i, permitting excitations of the form $i \rightarrow a$.

Subtracting the response of the core orbital density from that of the n-electron density (see Sec. S2 for details), leads to a eh-SIE-corrected n-electron response in terms of n–1-electron quantities

$$\begin{aligned} A_{ia,ib} &= F_{ab}^{(n-1)} - F_{ii}^{(n-1)}\delta_{ab} \\ &\quad + (ia|ib) + (1 - C_{\mathrm{HF}})(ia|f_{\mathrm{xc}}^{(n-1)}|ib) \\ B_{ia,ib} &= (ia|ib) + (1 - C_{\mathrm{HF}})(ia|f_{\mathrm{xc}}^{(n-1)}|ib) \end{aligned} \quad (10)$$

where,

$$f_{\mathrm{xc}}^{(n-1)} = \frac{\partial V_{\mathrm{xc}}[\rho^{(n-1)}]}{\partial \rho^{(n-1)}} \ . \quad (11)$$

Finally, we add this to the result of the initial response in Eq. 6 to obtain the working equations,

$$\begin{aligned} A_{ia,ib} &= F_{ab}^{(n-1)} + (ia|ib) + (1 - C_{\mathrm{HF}})(ia|f_{\mathrm{xc}}^{(n-1)}|ib) \\ B_{ia,ib} &= (ia|ib) + (1 - C_{\mathrm{HF}})(ia|f_{\mathrm{xc}}^{(n-1)}|ib) \end{aligned} \quad (12)$$

Each of the above responses comes from exact TDDFT, suggesting that with time-dependent exchange-correlation kernels this approach could be made exact

(to first order). Of course, knowledge of the exact functional would render this formalism obsolete because the exact functional is asymptotically correct (eh-SIE-free) and has frequency dependence (accounting for orbital relaxation).[69] From a utilitarian perspective, the exact functional is not available and all practical TDDFT implementations employ the adiabatic local density approximation (ALDA). Therefore, Eq. 12 can be viewed as a pragmatic correction to errors associated with the ALDA in TDDFT for XAS.

By nature of the core-ionized reference determinant and because the MOs do not relax on addition of the electron, the orbital relaxation codified into the n–1-electron density is retained. The second response is also eh-SIE-corrected, ensuring that there is no residual Coulomb-like interaction between excited electron and core hole. In fact, our proposed correction (Eq. S7) bears a delightful resemblance to the virtual-orbital self-interaction definition proposed by Imamura and Nakai,[70] with the added benefit that our equations capture orbital relaxation. This immediately suggests a metric for quantifying the extent of eh-SIE *via* the eigenvalues of the core-orbital response matrix (Eq. S9). In the limit of the Hartree-Fock functional ($C_{\mathrm{HF}} = 1$) this metric is exactly zero, and under the Tamm-Dancoff approximation (TDA)[71] Eq. 12 becomes precisely equivalent to the EA-CIS equation (Eq. 2). This implies that Eq. 12 is a generalization of EA-CIS to a DFT framework, so we call our approach electron-affinity TDDFT (EA-TDDFT).

In true analogy to EA-CIS, we will employ the TDA (EA-TDA) throughout this work, setting the $\mathbf{B}$ matrix to zero in Eq. 12. While in some applications the modified reference state (*e.g.* a core-ionized determinant) can lead to difficulties in solving the full non-Hermitian eigenvalue problem due to orbital rotations that drive the solution towards the ground state,[72–75] we have found that such problems are not encountered in EA-TDDFT.[76] Despite the fact that the full EA-TDDFT equations can be readily solved, the TDA is likely an excellent approximation within the confines of core excitations associated with K-edge XAS, as the elements of $\mathbf{B}$ are quite small. For the sake of comparison, EA-TDA is also a more direct analogue to STEX (a CIS theory), which is what we are attempting to generalize to DFT.

Apart from EA-TDA, we also consider the more naive approach of optimizing the orbitals of the n–1-electron system and using them directly to reconstruct the n-electron density. From this nonstationary initial state, we perform TDDFT under the TDA using the usual Casida formulation. In principle, this ion-orbital TDA (IO-TDA) approach incorporates orbital relaxation into the reference but lacks the ingredients that account for eh-SIE (details in Section S1).

It is important to note that EA-TDA differs strongly from IO-TDA in two respects. First, the energy of the intermediate n-electron state is constructed differently between the two methods. Whereas IO-TDA forms $E_{\mathrm{IO}}^{(n)}$, the energy of the n-electron Fock matrix using the orbitals of the core-ion with the core electron reattached, EA-TDA constructs $\tilde{E}^{(n)} = E^{(n-1)} + F_{ii}^{(n-1)}$. The two energies are only equivalent in the case of HF where the Fock matrix is strictly linear in the density. Second, we emphasize that Eq. 10 is not just a standard linear-response TDDFT expression, but one that encodes an exact first-order eh-SIE correction to the TDDFT equations. Without this correction, EA-TDA would correct for orbital relaxation but would not correct for the (even larger) self-interaction error in the excited state. The flowchart in Fig. 1 emphasizes the difference between the eigenvalues λ_p^{IO} of IO-TDA, which corrects for orbital relaxation but not eh-SIE, and the self-interaction corrected eigenvalues, λ_p, of EA-TDA. Later in this work, we investigate the impact of orbital relaxation and eh-SIE, showing that both must be adequately compensated for accurate results. Finally, we note that explicitly performing each step in the conceptual protocol in Fig. 1 is not necessary in practice, where Eq. 12 can be directly constructed and diagonalized to yield electron affinities γ_p such that $\omega_p = E^{(n-1)} + \gamma_p - E_0^{(n)}$.

This definition of the excitation energies is common between EA-TDA and STEX, but unlike STEX, EA-TDA does not use a projection operator to ensure orthogonal-

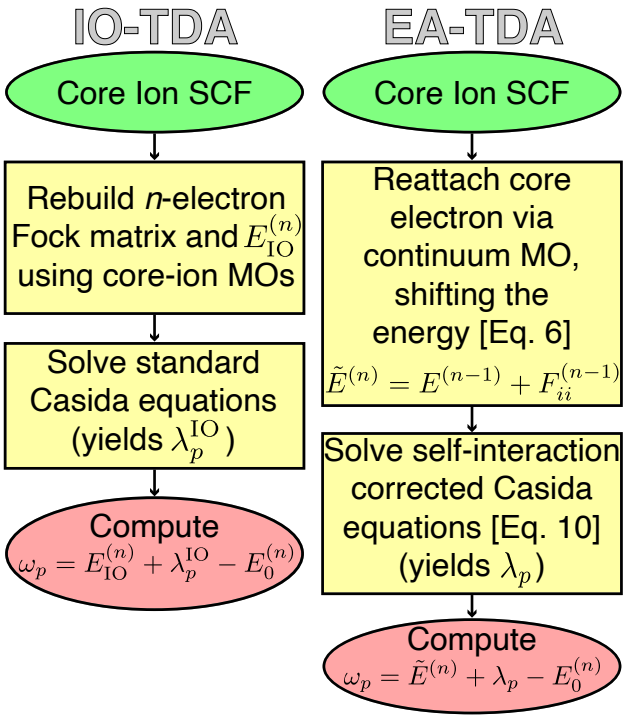

Figure 1. Flowchart describing the conceptual protocol for (left) an IO-TDA calculation and (right) an EA-TDA calculation, where $E_{\mathrm{IO}}^{(n)}$ is the energy of the n-electron Fock matrix constructed *via* core-ion orbitals, $E_0^{(n)}$ is the SCF ground-state energy, λ_p^{IO} are the eigenvalues of the Casida equations using the IO-TDA reference, λ_p are the eh-SIE corrected eigenvalues of EA-TDA, and ω_p are the core-excitation energies.

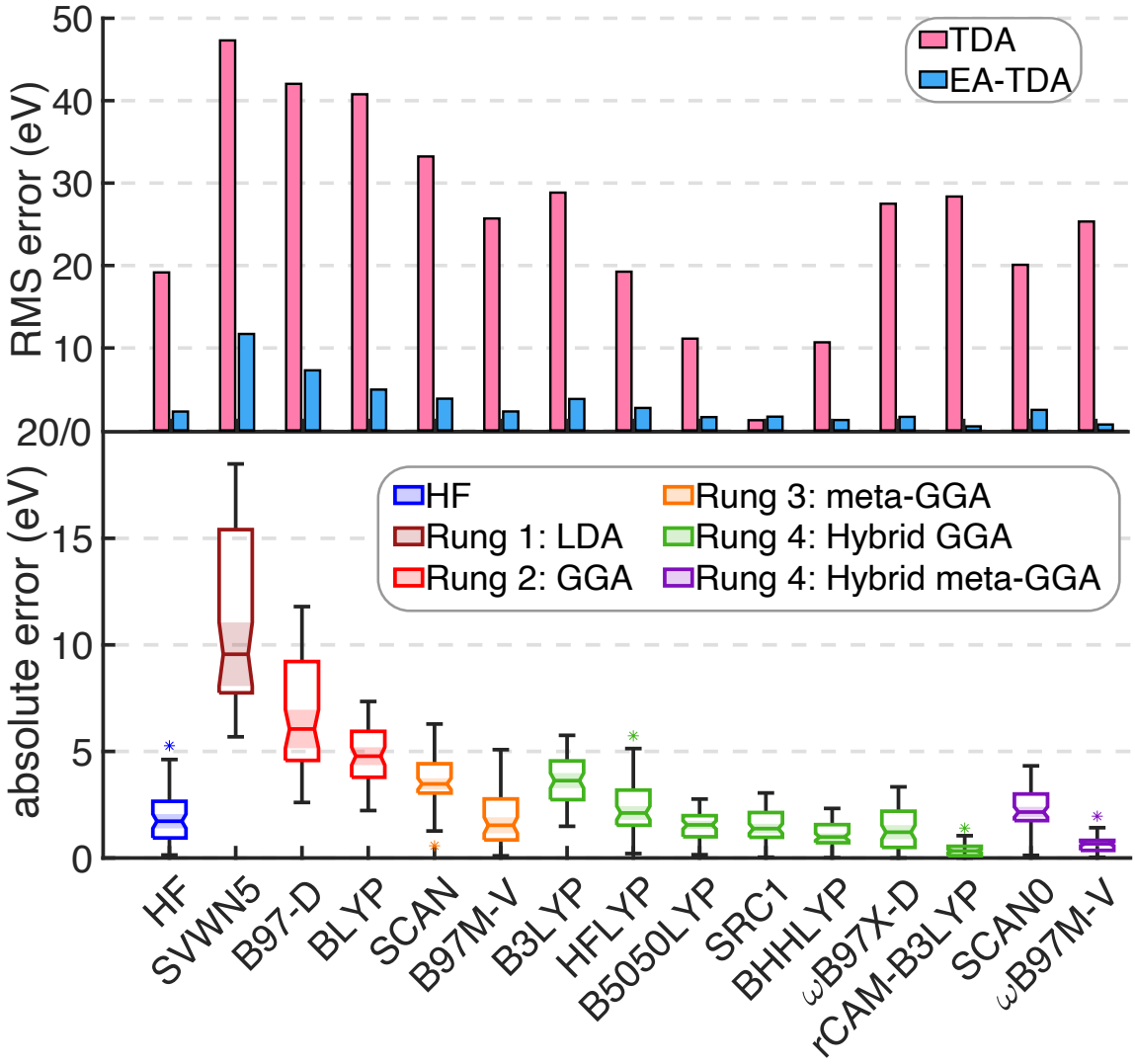

Figure 2. Absolute error statistics for 65 experimental K-edge transitions (lowest energy transition only). (Top) RMSE for standard TDA versus EA-TDA by functional. (Bottom) EA-TDA absolute error statistics. Upper and lower delimiters indicate maximum and minimum errors, respectively. Upper and lower bounds of each box are the upper and lower quartiles, respectively. Median absolute errors are indicated by horizontal lines and overlapping notches identify statistical similarities between distributions to the 95% confidence level. Outliers are indicated by asterisks. All calculations use aug-pcseg-1 for H and Br atoms and aug-pcX-2 otherwise.

ity between the singly-excited configurations and the n-electron ground state. Nonorthogonality can have detrimental effects on transition dipole moments (TDMs) even when energies are largely unaffected,[77] so we take it into account by using a pseudo-wavefunction *ansatz* (as done in TDDFT) to compute an overlap-free TDM (see Sec. S4 for details). We justify this approach by comparison of EA-TDA with the HF functional against STEX on a data set of 132 experimental K-edge transitions of small molecules. Tables S1–S3 reveal strong agreement between EA-TDA(HF) and STEX, with a maximum difference in transition energies of just 0.1 eV and a mean difference of 0.01 eV. The average difference between EA-TDA(HF) and STEX oscillator strengths is $\sim 10^{-5}$, with a maximum difference of $\sim 10^{-4}$ while the average STEX oscillator strength is 10^{-2}. We therefore conclude that the nonorthogonality of the final states in EA-TDA exerts a minimal influence on the details of the spectrum.

We assess the functional dependence of EA-TDA across 15 density functionals, and while not comprehensive we include data from local density approximation (LDA), generalized gradient approximation (GGA), meta-GGA, hybrid GGA, and hybrid meta-GGA functionals. The bottom panel of Fig. 2 indicates a clean recovery of the Jacob's Ladder concept in DFT, with errors decreasing with each step up through the rungs. Signed errors (Fig. S1) reveal that semi-local functionals tend to underestimate excitation energies, whereas asymptotically correct functionals exhibit very little systematic error. Increasing the fraction of exact exchange

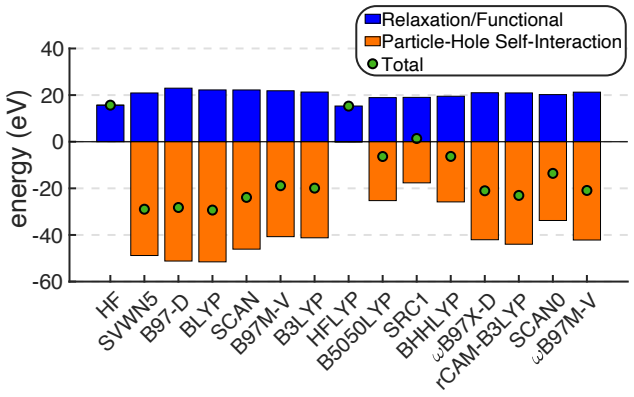

Figure 3. Error contributions to standard TDA that are corrected in EA-TDA, averaged over 65 K-edge transitions. The total (signed) error is taken to be the difference $Err(\text{TDA}) - Err(\text{EA-TDA})$, which is equivalent to the sum of the bars.

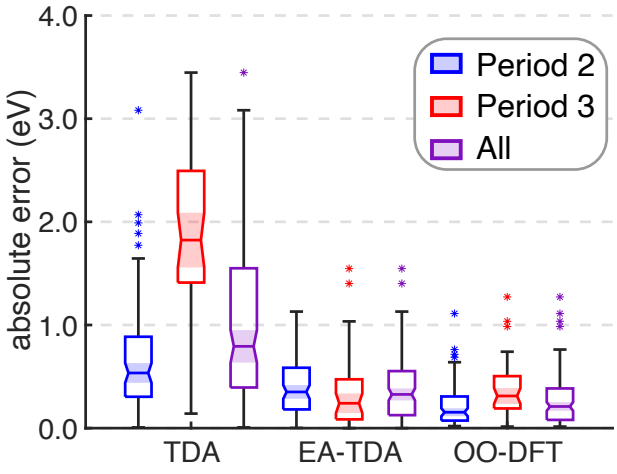

Figure 4. Absolute error statistics for the best method/functional combinations against 132 experimental K-edge transitions. Results are broken down by Period alongside the full data set. For TDA, SRC1-RX was used (where X = 1 or 2, depending on the period), rCAM-B3LYP and SCAN were used for EA-TDA and OO-DFT, respectively. All calculations use aug-pcseg-1 for H and Br and the doubly-augmented d-aug-pcX-2 basis otherwise.

improves error statistics up to a point with root mean squared error (RMSE) decreasing from BLYP to B3LYP and on to B5050LYP, but too much exact exchange degrades the results leading to higher RMSE for HFLYP than B5050LYP. Overall, asymptotically correct functionals perform best, and among them rCAM-B3LYP performs best of all with an RMSE of only 0.5 eV.

To understand the scope of the improvements offered by EA-TDA, we compare RMSEs of standard TDA with EA-TDA across functionals. The top panel of Fig. 2 reveals that for a given functional the average improvement offered by EA-TDA is on the order of tens of eV. In fact, the RMSE of rCAM-B3LYP improves by roughly two orders of magnitude, from 28.4 eV to 0.5 eV. This massive improvement is apparent in all but the SRC1 functional, which was parameterized specifically to cancel eh-SIE in standard TDDFT. This is a testament to the parameterization of SRC1, but the lack of improvement (or deterioration) of the results on switching to EA-TDA also exemplifies that eh-SIE is adequately quenched in EA-TDA.

On examination of Eq. 12 it becomes clear that a necessary criterion for a functional to perform well with EA-TDA is an accurate estimate of the electron affinity for each virtual MO. This is because the dominant term is $F_{ab}^{(n-1)}$, while the last two terms offer only small corrections to this energy because they are dependent on the overlap of the core orbital with the virtual MOs. Because asymptotically correct functionals perform best in the prediction of electron affinities,[78,79] so too do they perform best with EA-TDA.

The success of EA-TDA, a theory that takes orbital relaxation and eh-SIE into account, allows us to diagnose the origins of the errors in standard TDA. Using the metric defined in S9 we have immediate access to the amount of eh-SIE in standard TDA, while the remainder of the error in TDA can be ascribed to orbital relaxation effects. In Fig. 3, we define the total error (relaxation error plus eh-SIE) as the difference between standard TDA and EA-TDA, $Err(\text{TDA}) - Err(\text{EA-TDA})$, where the errors in excitation energies ω_{X} of a given method X are taken to be $Err(\text{X}) = \omega_{\text{X}} - \omega_{\text{ref}}$ with ω_{ref} representing the experimental value. Orbital relaxation contributes positive errors because without relaxation effects the predicted excitation energies are higher, whereas eh-SIE over-stabilizes the excitation energy due to a lack of particle-hole attraction, so its contribution is net negative.

The HF functional has zero contribution from eh-SIE because exact exchange yields correct particle-hole attraction. Similarly, HFLYP has a near-zero contribution from eh-SIE due to exact exchange, but it does not substantially improve upon HF in terms of orbital relaxation. Otherwise, the lion's share of error in most functionals comes from eh-SIE, with a relatively consistent contribution from a lack of orbital relaxation. An interesting exception to this rule is the SRC1 functional, which (owing to its parameterization for XAS) hosts a nearly optimal degree of error cancellation between orbital relaxation error and eh-SIE at a respective ratio of 52 : 48. Other functionals that benefit from near-cancellation of errors are those with a large fraction of global HF exchange such as B5050LYP and BHHLYP, which explains their notably better performance in comparison to other functionals in the top panel of Fig. 2. Overall, the largest contribution to the errors in TDA are from eh-SIE while orbital relaxation plays a consistent, strong, but auxiliary role in defining the total error.

We repeated the statistical analysis in Fig. 2 for IO-TDA and standard TDA to find the best functionals for each method (see Fig. S2 and Fig. S3 for de-

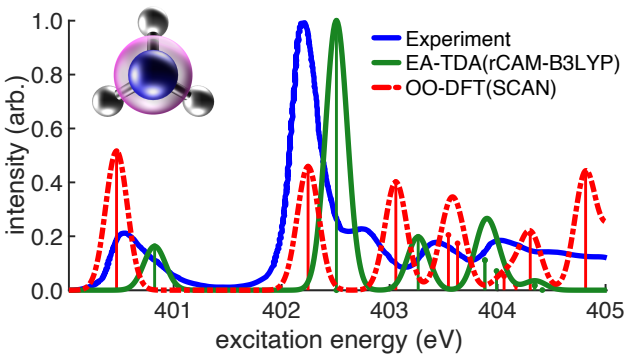

Figure 5. Ammonia K-edge X-ray absorption spectra for EA-TDA and OO-DFT juxtaposed against experimental data from Ref. 80. The aug-pcX-2 and aug-pcseg-1 basis sets were used for N and H, respectively.

tailed statistics). Our group has previously established SCAN as an excellent functional for core-excitations with OO-DFT, so we forego further analysis here.[44,45] The method/functional combinations that yielded the lowest errors on this test set were subjected to the more rigorous test of 132 experimental K-edge transitions of 46 molecules, ranging from 1–5 transitions per molecule. The results for IO-TDA were omitted because the best functional for IO-TDA was HF, suggesting that DFT provides no benefit to nonstationary TDA if eh-SIE is not properly taken into account. The results in Fig. 4 suggest that EA-TDA (RMSE = 0.5 eV) is almost as accurate as OO-DFT (RMSE = 0.4 eV) across the board, outperforming the SRC1 functionals used with standard TDA (RMSE = 1.3 eV) even though SRC1 was designed to accurately capture core-excitation energies.

EA-TDA also has excellent performance with respect to atomic size. While TDA and OO-DFT results show a statistically significant increase in errors from Period 2 elements to Period 3 (indicated by nonoverlapping notches in Fig. 4), EA-TDA results remain statistically similar with an RMSE that is equivalent to that of OO-DFT (0.5 eV). Admittedly, EA-TDA exhibits a slightly wider distribution of errors than OO-DFT, as shown by the quartiles. Being that the entire spectrum is obtained with one single EA-TDA calculation whereas OO-DFT optimizes specific configurations, this level of comparability between results is quite satisfactory.

The excellent comparability of EA-TDA and OO-DFT excitation energies begs the question: do transition properties also behave similarly? To investigate this, the experimental K-edge spectrum of ammonia is shown in Fig. 5 alongside calculated spectra using EA-TDA and OO-DFT. For this system, OO-DFT predicts slightly better excitation energies, whereas EA-TDA shows a slight (0.2 eV) blue shift. Insofar as transition strengths are concerned, the first major peak in the OO-DFT spectrum (normalized intensity of 0.52) corresponds to the 1s→3s transition, which is largely symmetry forbidden, leading to a small pre-edge peak in the experiment. The amplification of this feature is an artifact of ROKS, which allows strong singlet-triplet mixing when the initial and final states are isosymmetric.[81–85] Interestingly, the errors do not seem to stem from nonorthogonality of the ROKS states, as we account for residual nonorthogonality by subtracting the overlap-weighted nuclear dipole moment.[77] Instead, these errors may emerge as a direct consequence of spurious spatial symmetry-breaking due to use of approximate functionals.[86–88] Spuriously large oscillator strengths occur frequently for 1s→3s transitions in ROKS spectra, exerting a catastrophic impact on spectra containing truly dark 1s→3s transitions like the one in *trans*-butadiene (Fig. S4). The EA-TDA spectrum is devoid of such spurious high-intensity dark states and the overall qualitative nature of the spectrum is captured to high fidelity in all cases.

Overall, we find that EA-TDA successfully ameliorates eh-SIE, providing sizable improvements over TDDFT-based response theory, yielding core-excitation energies on par with OO-DFT while avoiding the spurious high-intensity dark states that occur in the latter. We anticipate that EA-TDA, with its low computational cost and high overall accuracy, will be a tool of great importance in condensed-phase systems. Our group is currently assessing the possibility of applying EA-TDA to liquid-phase XAS.[76]

Computational Details

All calculations were performed with a development version of the Q-Chem 5.4 software package.[89] The DFT calculations use a dense quadrature with 99 radial and 590 angular grid points to evaluate the exchange-correlation potential, and scalar relativistic effects are accounted for using a spin-free exact two-component (X2C) model.[45,90–97] Core-ionized references were optimized using restricted open-shell orbitals and the solutions were stabilized using combinations of maximum overlap method (MOM),[98,99] square-gradient minimization (SGM),[100] and state-targeted energy projection (STEP).[101] We use experimental molecular geometries whenever possible and all geometries are available in the Supporting Information.

Supporting Information

Additional details pertaining to the derivation presented including a description of IO-TDA, raw data comparing EA-TDA(HF) with STEX, signed error statistics of EA-TDA, absolute error statistics for IO-TDA and TDA, and spectra of *trans*-butadiene (PDF). All geometries used for K-edge XAS calculations (TXT).

Acknowledgements

This work was supported by the Director, Office of Science, Office of Basic Energy Sciences, of the U.S. Department of Energy under Contract No. DE-AC02-05CH11231.

[1] Buttersack, T. *et al.* Photoelectron spectra of alkali metal–ammonia microjets: From blue electrolyte to bronze metal. *Science* **2020,** *368,* 1086–1091.

[2] Gessner, O.; Gühr, M. Monitoring Ultrafast Chemical Dynamics by Time-Domain X-ray Photo- and Auger-Electron Spectroscopy. *Acc. Chem. Res.* **2016,** *49,* 138–145.

[3] Roth, F.; Borgwardt, M.; Wenthaus, L.; Mahl, J.; Palutke, S.; Brenner, G.; Mercurio, G.; Molodtsov, S.; Wurth, W.; Gessner, O.; Eberhardt, W. Direct observation of charge separation in an organic light harvesting system by femtosecond time-resolved XPS. *Nat. Commun.* **2021,** *12,* 1196.

[4] Katayama, T. *et al.* Tracking multiple components of a nuclear wavepacket in photoexcited Cu(I)-phenanthroline complex using ultrafast X-ray spectroscopy. *Nat. Commun.* **2019,** *10,* 3606.

[5] Zimmermann, P.; Peredkov, S.; Abdala, P. M.; DeBeer, S.; Tromp, M.; Müller, C.; van Bokhoven, J. A. Modern X-ray spectroscopy: XAS and XES in the laboratory. *Coord. Chem. Rev.* **2020,** *423,* 213466.

[6] Casida, M. E. Time-dependent density functional response theory for molecules. In *Recent Advances in Density Functional Methods, Part I*, Vol. I; Chong, D. P., Ed.; World Scientific: River Edge, NJ, 1995; Chapter 5, pages 155–192.

[7] Petersilka, M.; Gossmann, U. J.; Gross, E. K. U. Excitation energies from time-dependent density-functional theory. *Phys. Rev. Lett.* **1996,** *76,* 1212–1215.

[8] Bauernschmitt, R.; Ahlrichs, R. Treatment of electronic excitations within the adiabatic approximation of time dependent density functional theory. *Chem. Phys. Lett.* **1996,** *256,* 454–464.

[9] Furche, F. On the density matrix based approach to time-dependent density functional response theory. *J. Chem. Phys.* **2001,** *114,* 5982–5992.

[10] Marques, M. A. L.; Gross, E. K. U. Time-dependent density functional theory. *Annu. Rev. Phys. Chem.* **2004,** *55,* 427–455.

[11] Marques, M. A. L.; Maitra, N. T.; Nogueira, F. M. S.; Gross, E. K. U.; Rubio, A., Eds.; *Fundamentals of Time-Dependent Density Functional Theory;* volume 837 of *Lecture Notes in Physics* Springer: New York, 2012.

[12] Casida, M. E.; Huix-Rotllant, M. Progress in time-dependent density-functional theory. *Annu. Rev. Phys. Chem.* **2012,** *63,* 287–323.

[13] Burke, K.; Werschnik, J.; Gross, E. K. U. Time-dependent density functional theory: Past, present, and future. *J. Chem. Phys.* **2005,** *123,* 062206:1–9.

[14] Laurent, A. D.; Jacquemin, D. TD-DFT benchmarks: A review. *Int. J. Quantum Chem.* **2013,** *113,* 2019–2039.

[15] Lestrange, P. J.; Nguyen, P. D.; Li, X. Calibration of energy-specific TDDFT for modeling K-edge XAS spectra of light elements. *J. Chem. Theory Comput.* **2015,** *11,* 2994–2999.

[16] Chantzis, A.; Kowalska, J. K.; Maganas, D.; DeBeer, S.; Neese, F. *Ab initio* wave function-based determination of element specific shifts for the efficient calculation of x-ray absorption spectra of main group elements and first row transition metals. *J. Chem. Theory Comput.* **2018,** *14,* 3686–3702.

[17] Bussy, A.; Hutter, J. First-principles correction scheme for linear-response time-dependent density functional theory calculations of core electronic states. *J. Chem. Phys.* **2021,** *155,* 034108:1–10.

[18] Bussy, A.; Hutter, J. Efficient and low-scaling linear-response time-dependent density functional theory implementation for core-level spectroscopy of large and periodic systems. *Phys. Chem. Chem. Phys.* **2021,** *23,* 4736–4746.

[19] do Couto, P. C.; Hollas, D.; Slavíček, P. On the performance of optimally tuned range-separated hybrid functionals for x-ray absorption modeling. *J. Chem. Theory Comput.* **2015,** *11,* 3234–3244.

[20] Fransson, T.; Brumboiu, I. E.; Vidal, M. L.; Norman, P.; Coriani, S.; Dreuw, A. XABOOM: An x-ray absorption benchmark of organic molecules based on carbon, nitrogen, and oxygen 1s $\rightarrow \pi^*$ transitions. *J. Chem. Theory Comput.* **2021,** *17,* 1618–1637.

[21] Song, J.-W.; Watson, M. A.; Nakata, A.; Hirao, K. Core-excitation energy calculations with a long-range corrected hybrid exchange-correlation functional including a short-range Gaussian attenuation (LCgau-BOP). *J. Chem. Phys.* **2008,** *129,* 184113:1–9.

[22] Song, J.-W.; Watson, M. A.; Hirao, K. An improved long-range corrected hybrid functional with vanishing Hartree–Fock exchange at zero interelectronic distance (LC2gau-BOP). *J. Chem. Phys.* **2009,** *131,* 144108:1–9.

[23] Besley, N. A.; Peach, M. J. G.; Tozer, D. J. Time-dependent density functional theory calculations of near-edge x-ray absorption fine structure with short-range corrected functionals. *Phys. Chem. Chem. Phys.* **2009,** *11,* 10350–10358.

[24] Besley, N. A.; Asmuruf, F. A. Time-dependent density functional theory calculations of the spectroscopy of core electrons. *Phys. Chem. Chem. Phys.* **2010,** *12,* 12024–12039.

[25] Capano, G.; Penfold, T. J.; Besley, N. A.; Milne, C. J.; Reinhard, M.; Rittmann-Frank, H.; Glatzel, P.; Abela, R.; Rothlisberger, U.; Chergui, M.; Tavernelli, I. The role of Hartree–Fock exchange in the simulation of x-ray absorption spectra: A study of photoexcited $[Fe(bpy)_3]^{2+}$. *Chem. Phys. Lett.* **2013,** *580,* 179–184.

[26] Besley, N. A. Fast time-dependent density functional theory calculations of the x-ray absorption spectroscopy of large systems. *J. Chem. Theory Comput.* **2016,** *12,* 5018–5025.

[27] Besley, N. A. Density functional theory based methods for the calculation of x-ray spectroscopy. *Acc. Chem. Res.* **2020,** *53,* 1306–1315.

[28] Besley, N. A. Modeling of the spectroscopy of core electrons with density functional theory. *WIREs Comput. Mol. Sci.* **2021,** e1527:1–22.

[29] Roemelt, M.; Maganas, D.; DeBeer, S.; Neese, F. A combined DFT and restricted open-shell configuration interaction method including spin-orbit coupling: Application to transition metal L-edge x-ray absorption spectroscopy. *J. Chem. Phys.* **2013,** *138,* 204101:1–22.

[30] Maganas, D.; Roemelt, M.; Hävecker, M.; Trunschke, A.; Knop-Gericke, A.; Schlögl, R.; Neese, F. First principles calculations of the structure and V L-edge x-ray absorption spectra of V_2O_5 using local pair natural orbital coupled cluster theory and spin–orbit coupled configuration interaction approaches. *Phys. Chem. Chem. Phys.* **2013,** *15,* 7260–7276.

[31] Seidu, I.; Neville, S. P.; Kleinschmidt, M.; Heil, A.; Marian, C. M.; Schuurman, M. S. The simulation of x-ray absorption spectra from ground and excited electronic states using core-valence separated DFT/MRCI. *J. Chem. Phys.* **2019,** *151,* 144104:1–14.

[32] Slater, J. C.; Wood, J. H. Statistical exchange and the total energy of a crystal. *Int. J. Quantum Chem.* **1971,** *5,* 3–34.

[33] Slater, J. C. Statistical exchange-correlation in the self-consistent field. *Adv. Quantum Chem.* **1972,** *6,* 1–92.

[34] Stener, M.; Lisini, A.; Decleva, P. Density functional calculations of excitation energies and oscillator strengths for C1s $\rightarrow \pi^*$ and O1s $\rightarrow \pi^*$ excitations and ionization potentials in carbonyl containing molecules. *Chem. Phys.* **1995,** *191,* 141–154.

[35] Triguero, L.; Pettersson, L. G. M.; Ågren, H. Calculations of near-edge x-ray-absorption spectra of gas-phase and chemisorbed molecules by means of density-functional and transition-potential theory. *Phys. Rev. B* **1998,** *58,* 8097–8110.

[36] Triguero, L.; Pettersson, L. G. M.; Ågren, H. Calculations of x-ray emission spectra of molecules and surface adsorbates by means of density functional theory. *J. Phys. Chem. A* **1998,** *102,* 10599–10607.

[37] Cavalleri, M.; Odelius, M.; Nordlund, D.; Nilsson, A.; Pettersson, L. G. M. Half or full core hole in density functional theory x-ray absorption spectrum calculations of water? *Phys. Chem. Chem. Phys.* **2005,** *7,* 2854–2858.

[38] Leetmaa, M.; Ljungberg, M. P.; Lyubartsev, A.; Nilsson, A.; Pettersson, L. G. M. Theoretical approximations to x-ray absorption spectroscopy of liquid water and ice. *J. Electron Spectrosc.* **2010,** *177,* 135–157.

[39] Fransson, T.; Zhotobriukh, I.; Coriani, S.; Wikfeldt, K. T.; Norman, P.; Pettersson, L. G. M. Requirements of first-principles calculations of x-ray absorption spectra of liquid water. *Phys. Chem. Chem. Phys.* **2016,** *18,* 566–583.

[40] Michelitsch, G. S.; Reuter, K. Efficient simulation of near-edge x-ray absorption fine structure (NEXAFS) in density-functional theory: Comparison of core-level constraining approaches. *J. Chem. Phys.* **2019,** *150,* 074104:1–12.

[41] Jana, D.; Bandyopadhyay, B.; Mukherjee, D. Development and applications of a relaxation-inducing cluster expansion theory for treating strong relaxation and differential correlation effects. *Theor. Chem. Acc.* **1999,** *102,* 317–327.

[42] Rankine, C. D.; Penfold, T. J. Progress in the theory of x-ray spectroscopy: From quantum chemistry to machine learning and ultrafast dynamics. *J. Phys. Chem. A* **2021,** *125,* 4276–4293.

[43] Hait, D.; Head-Gordon, M. Orbital optimized density functional theory for electronic excited states. *J. Phys. Chem. Lett.* **2021,** *12,* 4517–4529.

[44] Hait, D.; Head-Gordon, M. Highly accurate prediction of core spectra of molecules at density functional theory cost: Attaining sub-electronvolt error from a restricted open-shell Kohn–Sham approach. *J. Phys. Chem. Lett.* **2020,** *11,* 775–786.

[45] Cunha, L. A.; Hait, D.; Kang, R.; Head-Gordon, M. Relativistic orbital-optimized density functional theory for accurate core-level spectroscopy. *J. Phys. Chem. Lett.* **2022,** *13,* 3438–3449.

[46] Dreuw, A.; Head-Gordon, M. Failure of time-dependent density functional theory for long-range charge-transfer excited-states: The zincbacteriochlorin–bacteriochlorin and bacteriochlorophyll–spheroidene complexes. *J. Am. Chem. Soc.* **2004,** *126,* 4007–4016.

[47] Dreuw, A.; Head-Gordon, M. Single-reference ab initio methods for the calculation of excited states of large molecules. *Chem. Rev.* **2005,** *105,* 4009–4037.

[48] Maitra, N. T. Undoing static correlation: Long-range charge transfer in time-dependent density-functional theory. *J. Chem. Phys.* **2005,** *122,* 234104:1–6.

[49] Hait, D.; Oosterbaan, K. J.; Carter-Fenk, K.; Head-Gordon, M. Computing X-ray absorption spectra from linear-response particles atop optimized holes. *J. Chem. Phys.* **2022,** *156,* 201104:1–9.

[50] Duchemin, I.; Deutsch, T.; Blase, X. Short-range to long-range charge-transfer excitations in the Zincbacteriochlorin-Bacteriochlorin complex: A Bethe-Salpeter study. *Phys. Rev. Lett.* **2012,** *109,* 167801:1–6.

[51] Jin, Y.; Yang, W. Excitation energies from single-particle Green's function with the *GW* approximation. *J. Phys. Chem. A* **2019,** *123,* 3199–3204.

[52] Fransson, T.; Dreuw, A. Simulating x-ray emission spectroscopy with algebraic diagrammatic construction schemes for the polarization propagator. *J. Chem. Theory Comput.* **2019,** *15,* 546–556.

[53] Dreuw, A.; Fransson, T. Using core-hole reference states for calculating X-ray photoelectron and emission spectra. *Phys. Chem. Chem. Phys.* **2022,** *24,* 11259–11267.

[54] Wilhelm, J.; Seewald, P.; Golze, D. Low-scaling *GW* with benchmark accuracy and application to phosphorene nanosheets. *J. Chem. Theory Comput.* **2021,** *17,* 1662–1677.

[55] Del Bene, J. E.; Ditchfield, R.; Pople, J. A. Self-consistent molecular orbital methods. X. Molecular orbital studies of excited states with minimal and extended basis sets. *J. Chem. Phys.* **1971,** *55,* 2236–2241.

[56] Foresman, J. B.; Head-Gordon, M.; Pople, J. A.; Frisch, M. J. Toward a systematic molecular orbital theory for excited states. *J. Phys. Chem.* **1992,** *96,* 135–149.

[57] Ågren, H.; Carravetta, V.; Vahtras, O.; Pettersson, L. G. M. Direct, atomic orbital, static exchange calculations of photoabsorption spectra of large molecules and clusters. *Chem. Phys. Lett.* **1994,** *222,* 75–81.

[58] Ågren, H.; Carravetta, V.; Vahtras, O.; Pettersson, L. G. M. Direct SCF direct static-exchange calculations of electronic spectra. *Theor. Chem. Acc.* **1997,** *97,* 14–40.

[59] Oosterbaan, K. J.; White, A. F.; Head-Gordon, M. Non-orthogonal configuration interaction with single substitutions for the calculation of core-excited states. *J. Chem.*

Phys. **2018,** *149,* 044116:1–7 Erratum: *ibid.* **149**, 139901:1–2 (2018).

[60] Oosterbaan, K. J.; White, A. F.; Head-Gordon, M. Non-orthogonal configuration interaction with single subsitutions for core-excited states: An extension to doublet radicals. *J. Chem. Theory Comput.* **2019,** *15,* 2966–2973.

[61] Oosterbaan, K. J.; White, A. F.; Hait, D.; Head-Gordon, M. Generalized single excitation configuration interaction: An investigation into the impact of the inclussion of non-orthogonality on the calculation of core-excited states. *Phys. Chem. Chem. Phys.* **2020,** *22,* 8182–8192.

[62] Liu, J.; Hättig, C.; Höfener, S. Analytical nuclear gradients for electron-attached and electron-detached states for the second-order algebraic diagrammatic construction scheme combined with frozen-density embedding. *J. Chem. Phys.* **2020,** *152,* 174109:1–15.

[63] Tsudeda, T.; Song, J.-W.; Suzuki, S.; Hirao, K. On Koopmans' theorem in density functional theory. *J. Chem. Phys.* **2010,** *133,* 174101:1–9.

[64] Fischer, S. A.; Cramer, C. J.; Govind, N. Excited state absorption from real-time time-dependent density functional theory. *J. Chem. Theory Comput.* **2015,** *11,* 4294–4303.

[65] Bowman, D. N.; Asher, J. C.; Fischer, S. A.; Cramer, C. J.; Govind, N. Excited-state absorption in tetrapyridy. porphyrins: Comparing real-time and quadratic-response time-dependent density functional theory. *Phys. Chem. Chem. Phys.* **2017,** *19,* 27452–27462.

[66] Cavaletto, S. M.; Nascimento, D. R.; Zhang, Y.; Govind, N.; Mukamel, S. Resonant stimulated x-ray raman spectroscopy of mixed-valence manganese complexes. *J. Phys. Chem. Lett.* **2021,** *12,* 5925–5931.

[67] Liekhus-Schmaltz, C. E.; Ho, P. J.; Weakly, R. B.; Aquila, A.; Schoelein, R. W.; Khalil, M.; Govind, N. Ultrafast x-ray pump x-ray probe transient absorption spectroscopy: A computational study and proposed experiment probing core?valence electronic correlations in solvated complexes. *J. Chem. Phys.* **2021,** *154,* 214107:1–9.

[68] Loe, C. M.; Liekhus-Schmaltz, C.; Govind, N.; Khalil, M. Spectral signatures of ultrafast excitedstate intramolecular proton transfer from computational multi-edge transient x-ray absorption spectroscopy. *J. Phys. Chem. Lett.* **2021,** *12,* 9840–9847.

[69] Maitra, N. T. Charge-transfer in time-dependent density functional theory. *J. Phys.: Condens. Matt.* **2017,** *29,* 423001:1–17.

[70] Imamura, Y.; Nakai, H. Analysis of self-interaction correction for describing core excited states. *Int. J. Quantum Chem.* **2007,** *107,* 23–29.

[71] Hirata, S.; Head-Gordon, M. Time-dependent density functional theory within the Tamm-Dancoff approximation. *Chem. Phys. Lett.* **1999,** *314,* 291–299.

[72] Goscinski, O.; Weiner, B. The role of algebraic formulations of approximate Green's Functions for systems with a finite number of electrons. *Phys. Scr.* **1980,** *21,* 385.

[73] Weiner, B.; Goscinski, O. Self-consistent approximation to the polarization propagator. *Int. J. Quantum Chem.* **1980,** *18,* 1109–1131.

[74] Prasad, M. D.; Pal, S.; Mukherjee, D. Some aspects of self-consistent propagator theories. *Phys. Rev. A* **1985,** *31,* 1287–1298.

[75] Datta, B.; Mukhopadhyay, D.; Mukherjee, D. Consistent propagator theory based on the extended coupled-cluster parametrization of the ground state. *Phys. Rev. A* **1993,** *47,* 3632–3648.

[76] Carter-Fenk, K.; Head-Gordon, M. On the choice of reference orbitals for linear-response calculations of solution-phase k-edge x-ray absorption spectra. **2022,** ChemRxiv. DOI: 10.26434/chemrxiv-2022-4w832.

[77] Worster, S. B.; Feighan, O.; Manby, F. R. Reliable transition properties from excited-state mean-field calculations. *J. Chem. Phys.* **2021,** *154,* 124106:1–9.

[78] Anderson, L. N.; Oviedo, M. B.; Wong, B. M. Accurate electron affinities and orbital energies of anions from a nonempirically tuned range-separated density functional theory approach. *J. Chem. Theory Comput.* **2017,** *13,* 1656–1666.

[79] Zhou, B.; Hu, Z.; Jiang, Y.; He, X.; Sun, Z.; Sun, H. Benchmark study of ionization potentials and electron affinities of armchair single-walled carbon nanotubes using density functional theory. *J. Phys.: Condens. Matter* **2018,** *30,* 215501.

[80] Schirmer, J.; Trofimov, A. B.; Randall, K. J.; Feldhaus, J.; Bradshaw, A. M.; Ma, Y.; Chen, C. T.; Sette, F. K-shell excitation of the water, ammonia, and methane molecules using high-resolution photoabsorption spectroscopy. *Phys. Rev. A* **1993,** *47,* 1136–1147.

[81] Grimm, S.; Nonnenberg, C.; Frank, I. Restricted open-shell Kohn–Sham theory for π–π transitions: I. Polyenes, cyanines, and protonated imines. *J. Chem. Phys.* **2003,** *119,* 11574–11584.

[82] Billeter, S. R.; Egli, D. Calculation of nonadiabatic couplings with restricted open-shell Kohn-Sham density-functional theory. *J. Chem. Phys.* **2006,** *125,* 224103:1–18.

[83] Filatov, M.; Shaik, S. Application of spin-restricted open-shell kohn–sham method to atomic and molecular multiplet states. *J. Chem. Phys.* **1999,** *110,* 116–125.

[84] Friedrichs, J.; Damianos, K.; Frank, I. Solving restricted open-shell equations in excited state molecular dynamics simulations. *Chem. Phys.* **2008,** *347,* 17–24.

[85] Kowalczyk, T.; Tsuchimochi, T.; Chen, P.-T.; Top, L.; Van Voorhis, T. Excitation energies and Stokes shifts from a restricted open-shell Kohn-Sham approach. *J. Chem. Phys.* **2013,** *138,* 164101:1–8.

[86] von Barth, U. Local-density theory of multiplet structure. *Phys. Rev. A* **1979,** *20,* 1693–1703.

[87] Görling, A. Symmetry in density-functional theory. *Phys. Rev. A* **1993,** *47,* 2783–2799.

[88] Levy, M.; Nagy, Á. Variational Density-Functional Theory for an Individual Excited State. *Phys. Rev. Lett.* **1999,** *83,* 4361–4364.

[89] Epifanovsky, E. *et al.* Software for the frontiers of quantum chemistry: An overview of developments in the Q-Chem 5 package. *J. Chem. Phys.* **2021,** *155,* 084801:1–59.

[90] Verma, P.; Derricotte, W. D.; Evangelista, F. A. Predicting near edge x-ray absorption spectra with the spin-free exact-two-component Hamiltonian and orthogonality constrained density functional theory. *J. Chem. Theory Comput.* **2016,** *12,* 144–156.

[91] Dyall, K. G. Interfacing relativistic and nonrelativistic methods. I. Normalized elimination of the small component in the modified Dirac equation. *J. Chem. Phys.* **1997,** *106,* 9618–9626.

[92] Kutzelnigg, W.; Liu, W. Quasirelativistic theory equivalent to fully relativistic theory. *J. Chem. Phys.* **2005,** *123,* 241102.

[93] Iliaš, M.; Saue, T. An infinite-order two-component relativistic Hamiltonian by a simple one-step transformation. *J. Chem. Phys.* **2007,** *126,* 064102.

[94] Liu, W.; Peng, D. Exact two-component Hamiltonians revisited. *J. Chem. Phys.* **2009,** *131,* 031104.

[95] Saue, T. Relativistic Hamiltonians for Chemistry: A Primer. *ChemPhysChem* **2011,** *12,* 3077–3094.

[96] Li, Z.; Xiao, Y.; Liu, W. On the spin separation of algebraic two-component relativistic Hamiltonians. *J. Chem. Phys.* **2012,** *137,* 154114.

[97] Cheng, L.; Gauss, J. Analytic energy gradients for the spin-free exact two-component theory using an exact block diagonalization for the one-electron Dirac Hamiltonian. *J. Chem. Phys.* **2011,** *135,* 084114.

[98] Gilbert, A. T. B.; Besley, N. A.; Gill, P. M. W. Self-consistent field calculations of excited states using the maximum overlap method (MOM). *J. Phys. Chem. A* **2008,** *112,* 13164–13171.

[99] Barca, G. M. J.; Gilbert, A. T. B.; Gill, P. M. W. Simple models for difficult electronic excitations. *J. Chem. Theory Comput.* **2018,** *14,* 1501–1509.

[100] Hait, D.; Head-Gordon, M. Excited state orbital optimization via minimizing the square of the gradient: General approach and application to singly and doubly excited states via density functional theory. *J. Chem. Theory Comput.* **2020,** *16,* 1699–1710.

[101] Carter-Fenk, K.; Herbert, J. M. State-targeted energy projection: A simple and robust approach to orbital relaxation of non-Aufbau self-consistent field solutions. *J. Chem. Theory Comput.* **2020,** *16,* 5067–5082.

Supporting Information for: "Electron-Affinity Time-Dependent Density Functional Theory: Formalism and Applications to Core-Excited States"

Kevin Carter-Fenk,*Leonardo A. Cunha,†Juan E. Arias-Martinez,‡and Martin Head-Gordon§
Kenneth S. Pitzer Center for Theoretical Chemistry,
Department of Chemistry, University of California, Berkeley, CA 94720, USA
Chemical Sciences Division, Lawrence Berkeley National Laboratory, Berkeley, CA 94720, USA

September 21, 2022

Contents

*carter-fenk@berkeley.edu
†leonardo.cunha@berkeley.edu
‡juanes@berkeley.edu
§mhg@cchem.berkeley.edu

S1 Linear-Response Time-Dependent Density Functional Theory and its Ion-Orbital Variant

The standard time-dependent density functional theory (TDDFT) orbital Hessians are used for the "ion-orbital" TDDFT approach, albeit from a nonstationary n-electron reference state that is constructed from the $n-1$-electron molecular orbitals (MOs) of the core-ionized system. The usual TDDFT **A** and **B** matrices take the form,

$$\begin{aligned} A_{ia,ib} &= E^{(n)}\delta_{ab} + F^{(n)}_{ab} - \varepsilon^{(n)}_{i}\delta_{ab} + (ia|ib) - C_{\mathrm{HF}}(ii|ab) + (1-C_{\mathrm{HF}})(ia|f^{(n)}_{\mathrm{xc}}|ib) \\ B_{ia,ib} &= (ia|ib) - C_{\mathrm{HF}}(ib|ai) + (1-C_{\mathrm{HF}})(ib|f^{(n)}_{\mathrm{xc}}|ai) \end{aligned} \tag{S1}$$

where $f^{(n)}_{\mathrm{xc}}$ is the exchange-correlation kernel, defined as,

$$f^{(n)}_{\mathrm{xc}} = \frac{\partial V_{\mathrm{xc}}[\rho^{(n)}]}{\partial \rho^{(n)}} \,, \tag{S2}$$

and where all quantities denoted with superscript (n) are computed using the n-electron density. In the case of IO-TDDFT, these n-electron quantities are constructed from the n-electron density built from the unrelaxed $n-1$-electron MOs of the core-ionized system:

$$P^{(n)}_{\mu\nu} = \sum_{i}^{N} C^{(n-1)}_{\mu i}(C^{(n-1)}_{\nu i})^{*} \tag{S3}$$

S2 Derivation of the $n-1$-electron Response Kernel

In order to correct for the particle-hole interaction error encountered in the intermediate n-electron state obtained after electron addition from the continuum MO, we take the response of the applied field on the n-electron state, which yields the Casida equations for the restricted case,

$$\begin{aligned} A^{(n)}_{ia,ib} &= E^{(n)}\delta_{ab} + F^{(n)}_{ab} - F^{(n)}_{ii}\delta_{ab} + 2(ia|ib) - C_{\mathrm{HF}}(ii|ab) + (1-C_{\mathrm{HF}})(ia|f^{(n)}_{\mathrm{xc}}|ib) \\ B^{(n)}_{ia,ib} &= 2(ia|ib) - C_{\mathrm{HF}}(ib|ai) + (1-C_{\mathrm{HF}})(ib|f^{(n)}_{\mathrm{xc}}|ai) \end{aligned} \tag{S4}$$

and subtract the response of the core orbital with associated the Fock matrix elements,

$$F^{\mathrm{CO}}_{pq} = F^{(n)}_{pq} - F^{(n-1)}_{pq} = (ii|pq) - C_{\mathrm{HF}}(ip|iq) + (1-C_{\mathrm{HF}})(p|V^{(n)}_{\mathrm{xc}} - V^{(n-1)}_{\mathrm{xc}}|q) \,, \tag{S5}$$

where $F^{(i)}_{pq}$ is the core electron's contribution to the Fock matrix of the n-electron system. This form of the Fock matrix accounts for all couplings between the core-electron components and the remainder of the n-electron density. The associated density matrix is idempotent and contains one electron in the core orbital, naturally constraining the excitations *via* the idemptency condition such that they can only emerge from core MO i. The response for the corresponding density matrix takes the form,

$$\begin{aligned} A^{\mathrm{CO}}_{ia,ib} &= E^{\mathrm{CO}}\delta_{ab} + F^{\mathrm{CO}}_{ab} - F^{\mathrm{CO}}_{ii}\delta_{ab} + \frac{\partial \mathbf{F}^{\mathrm{CO}}_{ia}}{\partial \mathbf{P}_{ib}} \\ B^{\mathrm{CO}}_{ia,ib} &= \frac{\partial \mathbf{F}^{\mathrm{CO}}_{ai}}{\partial \mathbf{P}_{ib}} \end{aligned} \,, \tag{S6}$$

where $E^{\mathrm{CO}} = \tilde{E}(n) - E_0(n-1)$ (the nonstationary n-electron energy minus the stationary $n-1$-electron energy of the core ion) and the partial derivatives yield the final expression for the core-orbital response,

$$\begin{aligned} A^{\mathrm{CO}}_{ia,ib} &= E^{\mathrm{CO}}\delta_{ab} + F^{\mathrm{CO}}_{ab} - F^{\mathrm{CO}}_{ii}\delta_{ab} + (ia|ib) - C_{\mathrm{HF}}(ii|ab) + (1-C_{\mathrm{HF}})(ia|f^{(n)}_{\mathrm{xc}} - f^{(n-1)}_{\mathrm{xc}}|ib) \\ B^{\mathrm{CO}}_{ia,ib} &= (ia|ib) + (1-C_{\mathrm{HF}})(ia|f^{(n)}_{\mathrm{xc}} - f^{(n-1)}_{\mathrm{xc}}|ib) \end{aligned} \,. \tag{S7}$$

Finally, subtracting the core-orbital part of the response from the full n-electron response leads to,

$$\begin{aligned} A^{(n)}_{ia,ib} - A^{\mathrm{CO}}_{ia,ib} &= E_0(n-1)\delta_{ab} + F^{(n-1)}_{ab} - F^{(n-1)}_{ii}\delta_{ab} + (ia|ib) + (1-C_{\mathrm{HF}})(ia|f^{(n-1)}_{\mathrm{xc}}|ib) \\ B^{(n)}_{ia,ib} - B^{\mathrm{CO}}_{ia,ib} &= (ia|ib) + (1-C_{\mathrm{HF}})(ia|f^{(n-1)}_{\mathrm{xc}}|ib) \end{aligned} \,. \tag{S8}$$

We note here that the energy E^{CO} is equal to the energy of orbital i only for the exact functional or Hartree-Fock theory, so the explicit form of this energy is never assumed.

S3 Long-Range Self-Interaction Metric

Within an ion-orbital *ansatz* such as IO-TDA, Eq. S7 is suggestive of a metric that can be used to quantify the degree of long-range self-interaction error (*i.e.* the degree of inexact particle-hole interaction) in approximate density functionals. Considering only the change in the excitation energy offered by the core-orbital correction, the total particle-hole interaction error for TDA approximations is,

$$A^{\mathrm{CO}}_{ia,ib} = F^{\mathrm{CO}}_{ab} - F^{\mathrm{CO}}_{ii}\delta_{ab} + (ia|ib) - C_{\mathrm{HF}}(ii|ab) + (1 - C_{\mathrm{HF}})(ia|f^{(n)}_{\mathrm{xc}} - f^{(n-1)}_{\mathrm{xc}}|ib) \tag{S9}$$

In Hartree-Fock theory Eq. S5 implies that $F^{\mathrm{CO}}_{ii} = 0$ and that $F^{\mathrm{CO}}_{ab} + (ia|ib) - (ii|ab) = 0$, resulting in a long-range self-interaction error of exactly zero. It also implies that IO-TDA with the HF functional should give equivalent results to STEX if the nonorthogonality with the n-electron ground state is not projected out of the STEX Hamiltonian. This is indeed the case, as IO-TDA and EA-TDA produce exactly the same results if the HF functional is used. If this metric produces a nonzero value, then the density functional approximation being used incurs some degree of inexact particle-hole interaction and the larger the value of the metric, the larger the long-range self-interaction error of the functional.

S4 Overlap-Free Transition Dipole Moments

The EA-TDA spectrum is comprised of states, $\{\Psi^a_i\}$, that are not orthogonal to the ground state reference, Φ_0, which must be considered when computing transition properties. Despite our double-linear-response formalism, we are only interested the usual transition dipole moments that are observed in one-dimensional x-ray spectroscopy. Nonorthogonality between excited state determinants and the ground state can have severely detrimental effects on transition moments,[15] but a simple fix is to subtract the overlap-weighted ground-state dipole moment from the transition dipole,

$$\vec{\mu} = \sum_a X^a_i \left(\langle \Phi_0 | \hat{\mu} | \Psi^a_i \rangle - \langle \Phi_0 | \hat{\mu} | \Phi_0 \rangle \langle \Phi_0 | \Psi^a_i \rangle \right) , \tag{S10}$$

where X^a_i are eigenvalues of the Tamm-Dancoff approximated Hermitian eigenvalue equation,

$$\mathbf{AX} = \omega \mathbf{X} . \tag{S11}$$

This is equivalent to translating the center of charge of the molecule to the origin prior to calculating the transition moments.

S5 Additional Data

Table S1: Difference between EA-TDA(HF) and STEX on 132 K-edge transitions: Be–N

Species	Atom	Transition	STEX[a]		EA-TDA[a]		ΔEnergy	ΔStrength
			Energy	Strength	Energy	Strength		
Be[b]	Be	1s→2p	115.814	9.08E−02	115.814	9.08E−02	0.000	0.00
CH_4[c]	C	1s→3s	287.303	0.00	287.323	0.00	0.019	0.00
CH_4[c]	C	1s→3p	288.441	6.30E−03	288.513	6.30E−03	0.072	1.00E−08
C_2H_2[d]	C	1s→ π^*	287.219	3.81E−02	287.225	3.81E−02	0.006	0.00
C_2H_2[d]	C	1s→3s	288.444	4.55E−04	288.461	4.79E−04	0.016	2.45E−05
C_2H_2[d]	C	1s→3p	289.492	9.82E−04	289.531	9.82E−04	0.039	0.00
C_2H_4[d]	C	1s→ π^*	286.419	4.27E−02	286.428	4.28E−02	0.010	1.03E−04
C_2H_4[d]	C	1s→3s	287.669	1.89E−03	287.695	1.99E−03	0.026	9.65E−05
C_2H_4[d]	C	1s→3p	288.263	3.48E−03	288.304	3.65E−03	0.041	1.70E−04
C_2H_6[d]	C	1s→3s	287.465	2.45E−03	287.487	2.52E−03	0.022	7.09E−05
C_2H_6[d]	C	1s→3p	288.334	4.73E−03	288.388	5.19E−03	0.054	4.60E−04
C_6H_6[d]	C	1s→ π^*	286.837	4.02E−02	286.835	4.02E−02	−0.003	−4.17E−05
C_6H_6[d]	C	1s→3s	287.812	2.16E−03	287.784	2.05E−03	−0.028	−1.06E−04
C_6H_6[d]	C	1s→3p	288.354	9.21E−04	288.320	9.31E−04	−0.034	1.06E−05
H_2CO[e]	C	1s→ π^*	288.041	5.94E−02	288.048	5.95E−02	0.007	6.33E−05
H_2CO[e]	C	1s→3s	291.305	4.18E−03	291.309	4.27E−03	0.004	8.80E−05
H_2CO[e]	C	1s→3p (b_2)	292.189	9.88E−03	292.219	1.01E−02	0.030	2.35E−04
H_2CO[e]	C	1s→3p (b_1)	292.429	2.56E−05	292.450	2.85E−05	0.022	2.87E−06
HFCO[f]	C	1s→ π^*	290.804	7.08E−02	290.808	7.09E−02	0.004	6.52E−05
HFCO[f]	C	1s→3s	294.246	8.72E−03	294.250	8.74E−03	0.004	2.74E−05
HFCO[f]	C	1s→3p	295.192	1.49E−03	295.197	1.52E−03	0.005	3.06E−05
HCOOH[g]	C	1s→ π^*	290.529	7.06E−02	290.533	7.07E−02	0.004	8.80E−05
HCOOH[g]	C	1s→3s	293.292	5.71E−03	293.302	5.91E−03	0.010	2.00E−04
HCOOH[g]	C	1s→3p	293.592	2.76E−03	293.602	2.68E−03	0.009	−7.42E−05
HCN[h]	C	1s→ π^*	288.098	4.63E−02	288.103	4.64E−02	0.005	3.99E−05
C_2N_2[h]	C	1s→ π_u^*	288.103	3.44E−02	288.103	3.44E−02	0.000	−1.00E−08
C_2N_2[h]	C	1s→3s	292.167	2.71E−04	292.166	2.82E−04	−0.001	1.13E−05
C_2N_2[h]	C	1s→ π_g^*/3p	293.187	4.72E−03	293.187	4.72E−03	0.000	0.00
CO[i]	C	1s→ π^*	289.125	7.77E−02	289.125	7.77E−02	0.000	0.00
CO[j]	C	1s→3s/σ	294.131	3.67E−03	294.127	3.68E−03	−0.004	1.04E−05
CO[j]	C	1s→3p/π	295.025	4.08E−03	295.025	4.08E−03	0.000	0.00
CO_2[k]	C	1s→ π_u^*	292.941	8.25E−02	292.941	8.25E−02	0.000	1.00E−08
CO_2[l]	C	1s→3s	295.276	0.00	295.269	0.00	−0.007	0.00
CO_2[l]	C	1s→3p	297.228	1.36E−03	297.228	1.36E−03	0.000	0.00
MeOH[m]	C	1s→3s	289.026	3.77E−03	289.044	3.77E−03	0.018	3.69E−06
butadiene[n]	C(t)	1s→ π^*	286.051	3.68E−02	286.056	3.68E−02	0.005	3.18E−05
butadiene[n]	C(c)	1s→ π^*	286.715	3.68E−02	286.717	3.68E−02	0.003	−7.55E−06
furan[o]	C (3 or 4)	1s→ π^*	287.490	3.16E−02	287.495	3.16E−02	0.004	3.98E−05
furan[o]	C (2 or 5)	1s→ π^*	288.160	4.24E−02	288.164	4.24E−02	0.003	2.97E−05
glycine[p]	C(CO)	1s→ π^*	290.885	7.32E−02	290.885	7.32E−02	0.000	2.95E−05
glycine[p]	C(sp3)	1s→ σ^*	289.222	4.10E−03	289.233	4.18E−03	0.011	8.60E−05
HCN[h]	N	1s→ π^*	400.857	4.29E−02	400.862	4.30E−02	0.005	5.14E−05
NH_3[c]	N	1s→3s	401.222	3.36E−03	401.226	3.37E−03	0.003	1.36E−05
NH_3[c]	N	1s→3p	402.702	8.56E−03	402.737	8.56E−03	0.035	0.00
NH_3[c]	N	1s→3p	403.387	5.99E−03	403.523	5.99E−03	0.136	−4.74E−06
N_2[i]	N	1s→ π^*	402.252	5.53E−02	402.252	5.53E−02	0.000	0.00
N_2O[l]	N(t)	1s→ π^*	402.300	4.61E−02	402.300	4.61E−02	0.000	0.00
N_2O[l]	N(t)	1s→3s/σ	405.630	1.68E−03	405.616	1.69E−03	−0.014	1.10E−05
N_2O[l]	N(t)	1s→3p/π	407.377	1.85E−03	407.377	1.85E−03	0.000	0.00
N_2O[l]	N(c)	1s→ π^*	406.062	5.99E−02	406.062	5.99E−02	0.000	−1.00E−08
N_2O[l]	N(c)	1s→3s/σ	410.517	2.11E−04	410.516	2.15E−04	−0.002	3.71E−06
N_2O[l]	N(c)	1s→3p/σ	412.007	1.34E−04	412.007	1.34E−04	0.000	0.00
C_2N_2[h]	N	1s→ π_u	400.150	3.62E−02	400.150	3.62E−02	0.000	0.00
C_2N_2[h]	N	1s→3s	404.379	5.90E−05	404.376	5.92E−05	−0.004	1.80E−07
C_2N_2[h]	N	1s→ π_g/3p	405.526	3.47E−04	405.526	3.47E−04	0.000	0.00
Imidazole[q]	N (CH=N-CH)	1s→ π^*	401.220	3.40E−02	401.222	3.40E−02	0.002	3.26E−05
Imidazole[q]	N (CH-NH-CH)	1s→ π^*	403.650	2.43E−02	403.654	2.43E−02	0.004	5.08E−05
pyrrole[r]	N	1s→ π^*	403.397	2.38E−02	403.402	2.39E−02	0.005	1.20E−04
glycine[p]	N (NH)	1s→ σ^*	401.922	2.73E−03	401.927	2.77E−03	0.004	4.35E−05
glycine[p]	N (NC)	1s→ π^*	402.761	4.67E−03	402.788	4.89E−03	0.028	2.24E−04

[a]aug-pcX-2 for non-H and non-Br atoms, aug-pcseg-1 otherwise. Data from: [b]Ref. 17, [c]Ref. 16, [d]Ref. 18, [e]Ref. 19, [f]Ref. 20, [g]Ref. 21, [h]Ref. 22, [i]Ref. 23, [j]Ref. 24, [k]Ref. 25, [l]Ref. 26, [m]Ref. 27, [n]Ref. 28, [o]Ref. 29, [p]Ref. 30, [q]Ref. 31, [r]Ref. 32

Table S2: Difference between EA-TDA(HF) and STEX on 132 K-edge transitions: O–Ne

Species	Atom	Transition	STEX[a]		EA-TDA[a]		ΔEnergy	ΔStrength
			Energy	Strength	Energy	Strength		
CO[b]	O	1s→ π^*	534.584	3.11E−02	534.584	3.11E−02	0.000	0.00
CO[c]	O	1s→3s/σ^*	538.608	8.71E−04	538.604	8.69E−04	−0.005	−2.35E−06
CO[c]	O	1s→3p/π^*	539.574	2.26E−05	539.570	8.40E−07	−0.004	−2.18E−05
CO_2[d]	O	1s→ π^*	536.345	2.57E−02	536.345	2.57E−02	0.000	−1.00E−08
CO_2[d]	O	1s→3s	536.619	2.57E−03	536.606	2.58E−03	−0.013	1.07E−05
CO_2[e]	O	1s→3p/π_u^*	538.751	3.44E−05	538.751	3.44E−05	0.000	0.00
CO_2[e]	O	1s→3p/σ^*	539.051	1.53E−03	539.050	1.52E−03	−0.001	−6.25E−06
MeOH[f]	O	1s→ σ^*	534.543	6.25E−03	534.547	6.27E−03	0.004	1.62E−05
H_2CO[g]	O	1s→ π^*	531.745	3.69E−02	531.747	3.69E−02	0.002	4.57E−05
H_2CO[g]	O	1s→3s	535.045	5.46E−04	535.062	5.48E−04	0.017	2.13E−06
H_2CO[g]	O	1s→3p	535.978	1.16E−05	535.992	4.55E−05	0.014	3.40E−05
HCFO[h]	O	1s→ π^*	533.115	3.49E−02	533.118	3.49E−02	0.002	3.51E−05
HCFO[h]	O	1s→3s	536.817	6.47E−04	536.822	6.22E−04	0.005	−2.47E−05
HCFO[h]	O	1s→3p	537.142	1.93E−03	537.151	1.98E−03	0.009	5.62E−05
HCOOH[f]	O (CO)	1s→ π^*	533.189	3.07E−02	533.192	3.08E−02	0.003	6.54E−05
HCOOH[f]	O (OH)	1s→ π^*/3s	536.361	7.86E−03	536.360	7.87E−03	−0.001	4.09E−06
H_2O[i]	O	1s→3s	534.399	7.46E−03	534.398	7.37E−03	−0.001	−9.52E−05
H_2O[i]	O	1s→3p	536.086	1.35E−02	536.110	1.33E−02	0.024	−1.95E−04
N_2O[d]	O	1s→ π^*	535.211	1.88E−02	535.211	1.88E−02	0.000	1.00E−08
N_2O[d]	O	1s→3s/σ^*	537.223	3.31E−03	537.209	3.35E−03	−0.014	4.24E−05
N_2O[d]	O	1s→3p/π^*	538.930	1.57E−03	538.930	1.57E−03	0.000	0.00
glycine[j]	O (CO)	1s→ π^*	533.775	3.02E−02	533.774	3.02E−02	−0.001	3.70E−05
glycine[j]	O (OH)	1s→ σ^*	536.307	7.00E−03	536.306	7.04E−03	−0.001	3.58E−05
HCFO[h]	F	1s→ π^*	688.940	8.69E−03	688.943	8.70E−03	0.003	1.08E−05
HF[k]	F	1s→ σ^*	687.533	1.34E−02	687.539	1.34E−02	0.006	−3.42E−05
HF[k]	F	1s→3p/σ^*	690.955	6.39E−03	691.037	6.94E−03	0.082	5.48E−04
F_2[k]	F	1s→ σ_u	684.087	5.18E−02	684.076	5.18E−02	−0.010	−5.61E−05
F_2[k]	F	1s→3s	693.333	9.40E−04	693.333	9.14E−04	−0.001	−2.64E−05
F_2[k]	F	1s→3p	693.557	2.15E−03	693.557	2.15E−03	0.000	0.00
Ne[†,l]	Ne	1s→3s	864.931	0.00	864.923	0.00	−0.008	0.00
Ne[†,l]	Ne	1s→3p	866.679	3.15E−03	866.679	2.48E−03	0.000	−6.71E−04

[a]aug-pcX-2 for non-H and non-Br atoms, aug-pcseg-1 otherwise.
[†]Doubly-augmented d-aug-pcX-3 basis due to large basis set incompleteness errors
Data from: [b]Ref. 23, [c]Ref. 24, [d]Ref. 26, [e]Ref. 33, [f]Ref. 21, [g]Ref. 19, [h]Ref. 20, [i]Ref. 16, [j]Ref. 30, [k]Ref. 34, [l]Ref. 35

Table S3: Difference between EA-TDA(HF) and STEX on 132 K-edge transitions: Si–Cl

Species	Atom	Transition	STEX[a]		EA-TDA[a]		ΔEnergy	ΔStrength
			Energy	Strength	Energy	Strength		
SiH_4[b]	Si	1s→t2	1845.109	1.59E−03	1845.132	1.56E−03	0.023	−3.40E−05
SiH_4[b]	Si	1s→4p	1845.860	1.02E−03	1845.882	1.18E−03	0.021	1.61E−04
SiF_4[b]	Si	1s→a1	1849.793	0.00	1849.785	0.00	−0.008	0.00
SiF_4[b]	Si	1s→t2	1851.330	8.73E−04	1851.330	8.73E−04	0.000	0.00
SiF_4[b]	Si	1s→4p	1852.743	4.17E−03	1852.743	4.17E−03	0.000	0.00
$SiCl_4$[b]	Si	1s→a1	1848.188	0.00	1848.171	0.00	−0.018	0.00
$SiCl_4$[b]	Si	1s→t2	1849.331	5.53E−03	1849.331	5.53E−03	0.000	0.00
$SiBr_4$[b]	Si	1s→a1	1846.973	0.00	1846.993	0.00	0.020	0.00
$SiBr_4$[b]	Si	1s→t2	1848.593	5.57E−03	1848.593	5.57E−03	0.000	0.00
PH_3[c]	P	1s→ σ^*	2148.203	5.84E−04	2148.208	5.89E−04	0.005	4.81E−06
PF_3[c]	P	1s→ σ^*	2152.812	6.60E−03	2152.812	6.60E−03	0.000	0.00
PF_5[c]	P	1s→ σ^*	2159.064	4.39E−03	2159.064	4.39E−03	0.000	0.00
POF_3[c]	P	1s→ σ^*	2157.270	4.95E−03	2157.270	4.95E−03	0.000	1.00E−08
H_2S[d]	S	1s→ σ^*	2475.231	1.28E−03	2475.236	1.28E−03	0.005	−3.03E−06
H_2S[d]	S	1s→Ry	2477.071	8.87E−05	2477.183	6.19E−05	0.112	−2.68E−05
CS_2[e]	S	1s→$2\pi_u$	2473.461	2.55E−03	2473.461	2.55E−03	0.000	0.00
CS_2[e]	S	1s→$3\sigma_g/3\sigma_u$	2476.323	1.22E−05	2476.321	1.24E−05	−0.002	1.10E−07
SF_4[f]	S	1s→b_2^*	2481.921	8.83E−03	2481.921	8.83E−03	0.000	0.00
SF_4[f]	S	1s→a_1^*	2484.905	4.82E−03	2484.886	4.82E−03	−0.018	−6.42E−06
SF_4[f]	S	1s→b_1^*	2485.866	1.01E−02	2485.866	1.01E−02	0.000	0.00
SF_6[d]	S	1s→ σ^* (a_1)	2487.304	0.00	2487.267	0.00	−0.037	0.00
SF_6[d]	S	1s→ σ^* (t)	2490.756	1.56E−03	2490.756	1.56E−03	0.000	1.00E−08
SO_2[d]	S	1s→ σ^* (b1)	2476.306	8.39E−03	2476.286	8.37E−03	−0.020	−1.90E−05
SO_2[d]	S	1s→ σ^* (a1)	2481.978	2.58E−03	2481.977	2.58E−03	−0.002	2.80E−07
SO_2[d]	S	1s→ σ^* (b2)	2482.856	2.31E−03	2482.856	2.31E−03	0.000	0.00
SCO[e]	S	1s→3π	2474.910	2.38E−03	2474.945	2.38E−03	0.034	8.91E−06
SCO[e]	S	1s→5σ	2476.277	8.34E−04	2476.272	8.36E−04	−0.005	1.89E−06
SCO[e]	S	1s→6σ	2477.339	1.17E−03	2477.339	1.17E−03	−0.001	−3.82E−06
SF_5Cl[g]	S	1s→ σ^*	2484.815	9.44E−04	2484.793	9.23E−04	−0.021	−2.05E−05
SF_5Cl[g]	S	1s→ σ^*	2488.638	6.67E−03	2488.631	6.71E−03	−0.007	4.04E−05
SF_5Cl[g]	S	1s→ σ^*	2489.517	1.12E−04	2489.516	1.09E−04	−0.001	−2.71E−06
HCl[h]	Cl	1s→3p σ^*	2826.188	2.95E−03	2826.184	2.94E−03	−0.004	−2.03E−06
HCl[h]	Cl	1s→4s σ	2828.593	1.06E−03	2828.593	1.06E−03	0.000	9.70E−07
HCl[h]	Cl	1s→4p π/4p σ	2829.288	1.62E−04	2829.287	1.62E−04	−0.001	5.60E−07
Cl_2[h]	Cl	1s→$3p/\sigma_u^*$	2823.962	5.58E−03	2823.959	5.58E−03	−0.003	−4.35E−06
Cl_2[h]	Cl	1s→4p/3d	2829.889	6.51E−04	2829.888	6.52E−04	−0.002	1.14E−06
CH_3Cl[i]	Cl	1s→a_1	2826.649	2.29E−03	2826.652	2.31E−03	0.002	1.82E−05
CH_3Cl[i]	Cl	1s→Ry	2827.995	1.57E−04	2828.063	1.70E−04	0.068	1.22E−05
SF_5Cl[g]	Cl	1s→ σ^*	2825.235	4.49E−03	2825.233	4.49E−03	−0.002	−3.67E−06
SF_5Cl[g]	Cl	1s→4p	2829.231	4.91E−04	2829.230	4.93E−04	−0.001	1.88E−06
CCl_3F[i]	Cl	1s→e	2826.865	3.38E−03	2826.863	3.37E−03	−0.002	−3.19E−06

[a]aug-pcX-2 for non-H and non-Br atoms, aug-pcseg-1 otherwise.
Data from: [b]Ref. 36, [c]Ref. 37, [d]Ref. 38, [e]Ref. 39, [f]Ref. 40, [g]Ref. 41, [h]Ref. 42, [i]Ref. 43

Table S4: Difference between EA-TDA(HF) and STEX transition dipole moments[a] on 65 K-edge transitions: Be–N

Species	Atom	Transition	$\Delta\mu_x$	$\Delta\mu_y$	$\Delta\mu_z$
Be	Be	1s→2p	−2.53E−06	2.55E−03	9.42E−04
CH_4	C	1s→3s	0.000	0.000	0.000
C_2H_2	C	1s→ π^*	−2.45E−03	4.87E−04	0.000
C_2H_4	C	1s→ π^*	0.000	0.000	0.000
C_2H_6	C	1s→3s	0.000	3.00E−08	9.29E−06
C_6H_6	C	1s→ π^*	0.000	0.000	0.000
H_2CO	C	1s→ π^*	0.000	0.000	0.000
HFCO	C	1s→ π^*	0.000	0.000	0.000
HCOOH	C	1s→ π^*	0.000	0.000	0.000
HCN	C	1s→ π^*	1.58E−03	−8.48E−05	0.000
C_2N_2	C	1s→ π_u^*	−1.49E−02	3.88E−03	0.000
CO	C	1s→ π^*	8.98E−04	−1.68E−05	0.000
CO_2	C	1s→ π_u^*	−1.91E−03	1.48E−03	0.000
MeOH	C	1s→3s	−3.82E−05	−1.26E−04	0.000
butadiene	C(t)	1s→ π^*	0.000	0.000	0.000
butadiene	C(c)	1s→ π^*	7.14E−06	0.000	6.34E−05
furan	C (3 or 4)	1s→ π^*	0.000	0.000	0.000
furan	C (2 or 5)	1s→ π^*	0.000	0.000	0.000
glycine	C(CO)	1s→ π^*	0.000	0.000	0.000
glycine	C(sp3)	1s→ σ^*	1.83E−05	−6.31E−05	0.000
HCN	N	1s→ π^*	−1.05E−03	2.29E−05	0.000
NH_3	N	1s→3s	0.000	0.000	2.68E−05
N_2	N	1s→ π^*	8.01E−03	−9.65E−04	0.000
N_2O	N(t)	1s→ π^*	−2.00E−02	1.26E−02	0.000
N_2O	N(c)	1s→ π^*	6.48E−03	−2.43E−03	0.000
C_2N_2	N	1s→ π_u	−1.69E−02	5.55E−03	0.000
Imidazole	N (CH=N-CH)	1s→ π^*	5.96E−06	6.12E−05	0.000
Imidazole	N (CH-NH-CH)	1s→ π^*	0.000	0.000	−1.00E−08
pyrrole	N	1s→ π^*	0.000	0.000	6.49E−05
glycine	N (NH)	1s→ σ^*	2.70E−05	−3.74E−05	0.000
CO	O	1s→ π^*	2.04E−04	−4.13E−06	0.000
CO_2	O	1s→ π^*	5.91E−04	−9.88E−05	0.000
MeOH	O	1s→ σ^*	3.77E−05	−5.72E−05	0.000
H_2CO	O	1s→ π^*	0.000	0.000	0.000
HCFO	O	1s→ π^*	0.000	0.000	0.000
HCOOH	O (CO)	1s→ π^*	3.13E−05	−4.02E−06	0.000
HCOOH	O (OH)	1s→ π^*/3s	0.000	0.000	0.000
H_2O	O	1s→3p	0.000	0.000	3.03E−05
N_2O	O	1s→3s/σ^*	9.17E−03	−2.35E−03	0.000
glycine	O (CO)	1s→ π^*	2.83E−05	1.55E−05	0.000
glycine	O (OH)	1s→ σ^*	0.000	0.000	0.000
HCFO	F	1s→ π^*	0.000	0.000	0.000
HF	F	1s→ σ^*	0.000	0.000	7.75E−06
F_2	F	1s→3s	0.000	0.000	−2.10E−05
Ne[†]	Ne	1s→3p	0.000	0.000	0.000
SiH_4	Si	1s→t2	0.000	0.000	0.000
SiF_4	Si	1s→a1	0.000	0.000	0.000
$SiCl_4$	Si	1s→a1	0.000	0.000	0.000
$SiBr_4$	Si	1s→a1	0.000	0.000	0.000
PH_3	P	1s→ $\sigma*$	0.000	−2.00E−08	6.80E−07
PF_3	P	1s→ σ^*	−8.00E−08	0.000	0.000
PF_5	P	1s→ σ^*	0.000	−1.00E−08	0.000
POF_3	P	1s→ σ^*	0.000	0.000	1.41E−05
H_2S	S	1s→ σ^*	0.000	0.000	5.50E−07
CS_2	S	1s→$2\pi_u$	1.89E−04	−1.94E−05	0.000
SF_4	S	1s→b_2^*	0.000	0.000	0.000
SF_6	S	1s→ σ^* (a_1)	0.000	0.000	0.000
SO_2	S	1s→ σ^* (b1)	0.000	0.000	0.000
SCO	S	1s→3π	−1.79E−04	3.43E−05	0.000
SF_5Cl	S	1s→ σ^*	0.000	0.000	−3.04E−05
HCl	Cl	1s→3p σ^*	0.000	0.000	−1.59E−06
Cl_2	Cl	1s→4p/3d	0.000	0.000	−2.47E−06
CH_3Cl	Cl	1s→a_1	0.000	0.000	2.00E−06
SF_5Cl	Cl	1s→ σ^*	0.000	0.000	−2.33E−06
CCl_3F	Cl	1s→e	0.000	−2.39E−06	−7.00E−08

[a]aug-pcX-2 for non-H and non-Br atoms, aug-pcseg-1 otherwise. $\Delta\mu_p = \mu_p^{\text{EA-TDA}} - \mu_p^{\text{STEX}}$.
[†]Doubly-augmented d-aug-pcX-3 basis due to large basis set incompleteness errors

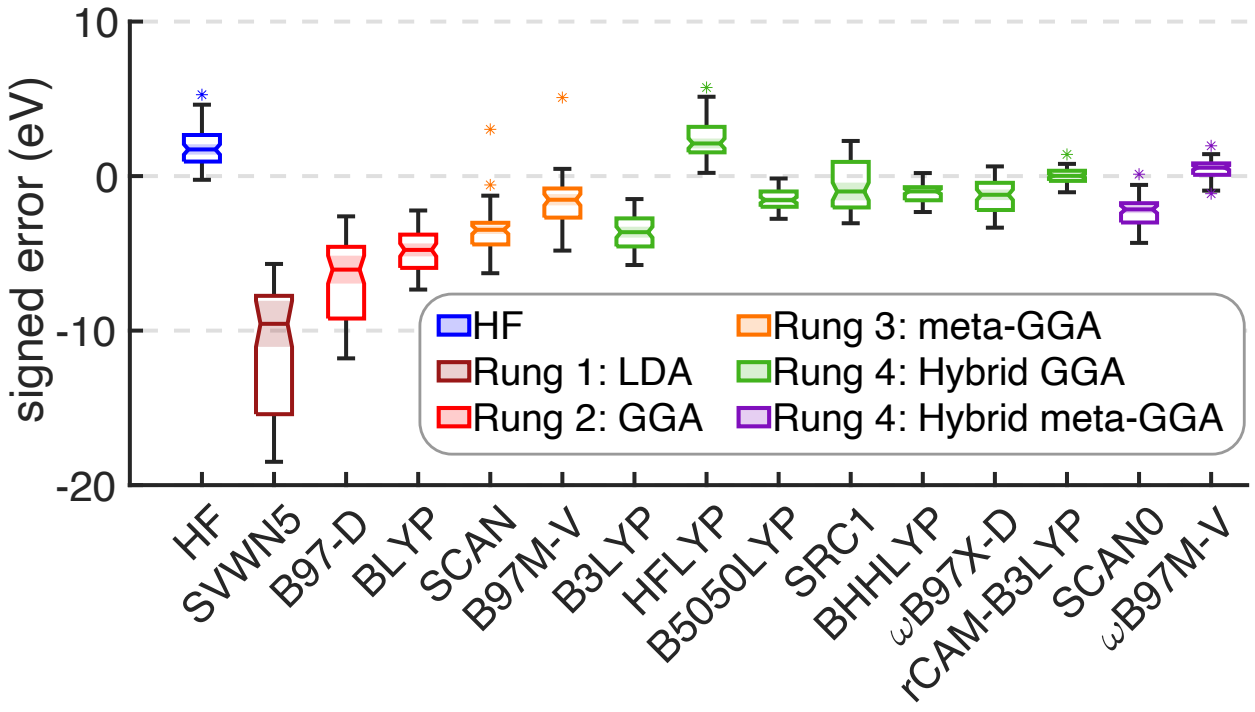

Figure S1: EA-TDA signed error statistics for 65 experimental K-edge transitions (lowest energy transition only). The aug-pcseg-1 basis was used for H and Br, aug-pcX-2 for all other atoms. A negative sign indicates an underestimation in the excitation energy. Upper and lower delimiters indicate maximum and minimum errors, respectively. Upper and lower bounds of each box are the upper and lower quartiles, respectively. Median absolute errors are indicated by horizontal lines and overlapping notches identify statistical similarities between distributions to the 95% confidence level. Outliers are indicated by asterisks.

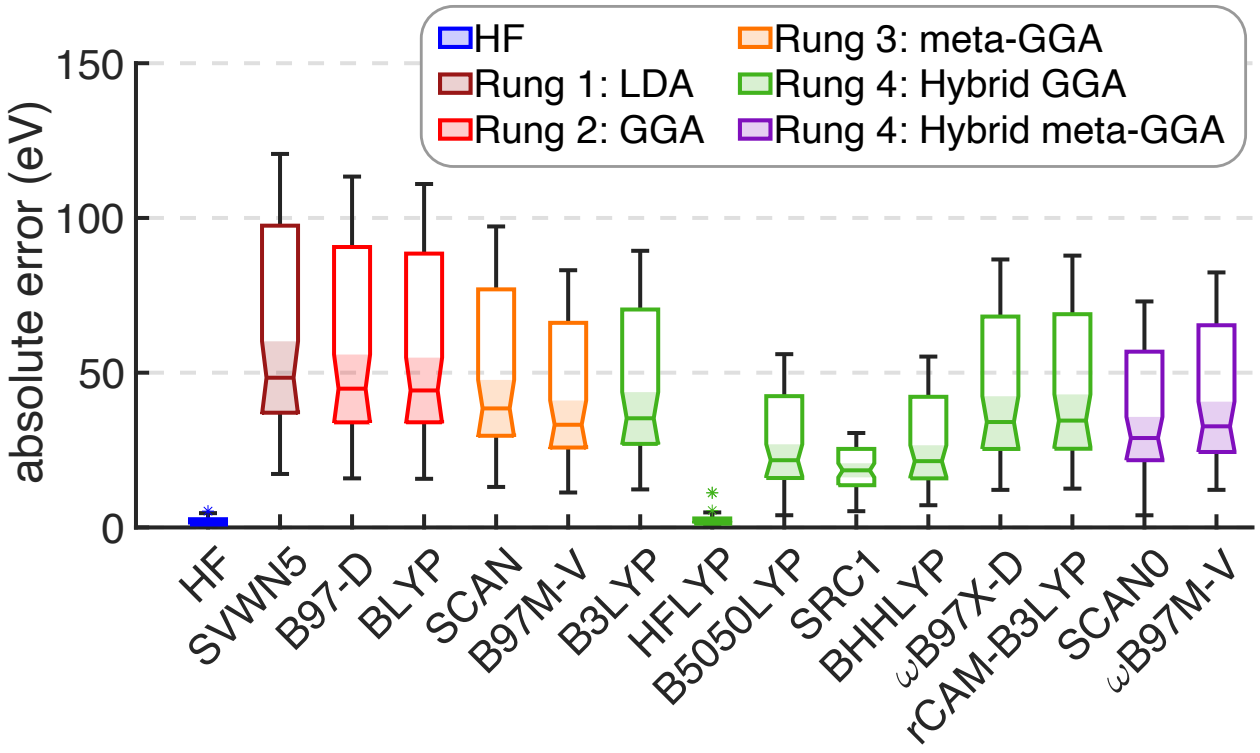

Figure S2: IO-TDA absolute error statistics for 65 experimental K-edge transitions (lowest energy transition only). The aug-pcseg-1 basis was used for H and Br, aug-pcX-2 for all other atoms. Upper and lower delimiters indicate maximum and minimum errors, respectively. Upper and lower bounds of each box are the upper and lower quartiles, respectively. Median absolute errors are indicated by horizontal lines and overlapping notches identify statistical similarities between distributions to the 95% confidence level. Outliers are indicated by asterisks.

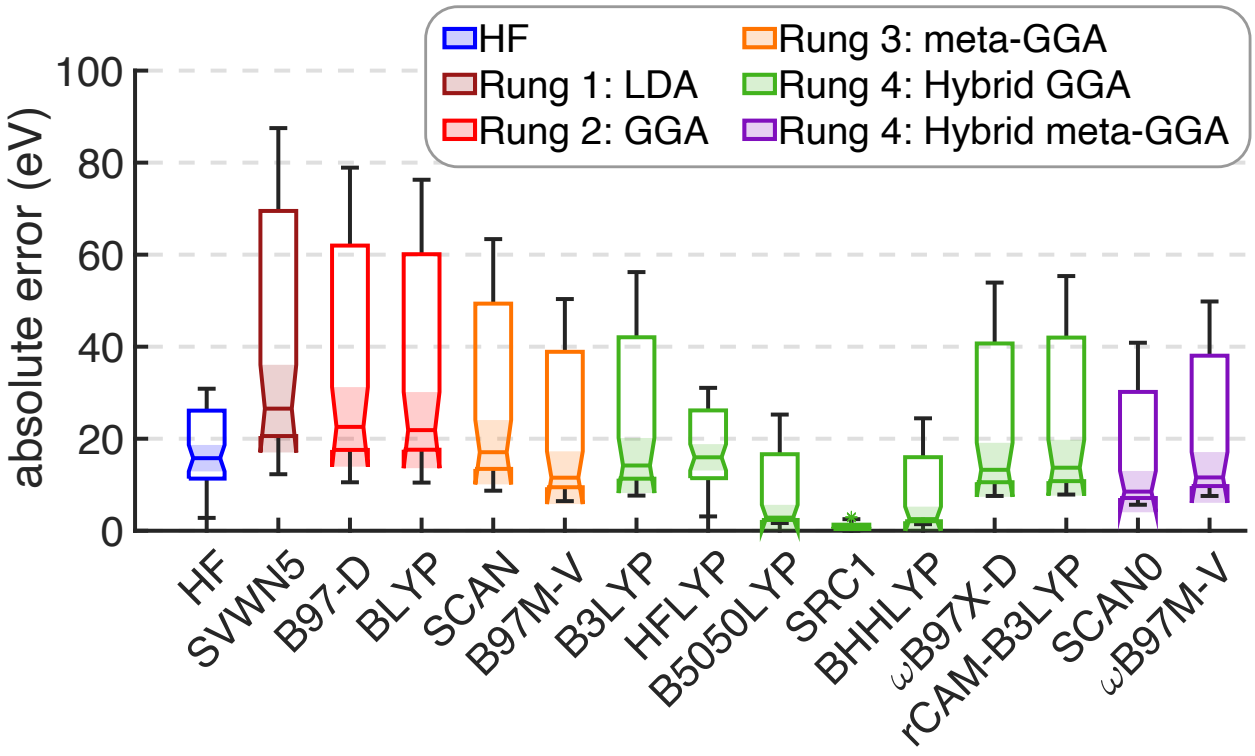

Figure S3: Standard TDA absolute error statistics for 65 experimental K-edge transitions (lowest energy transition only). The aug-pcseg-1 basis was used for H and Br, aug-pcX-2 for all other atoms. Upper and lower delimiters indicate maximum and minimum errors, respectively. Upper and lower bounds of each box are the upper and lower quartiles, respectively. Median absolute errors are indicated by horizontal lines and overlapping notches identify statistical similarities between distributions to the 95% confidence level. Outliers are indicated by asterisks.

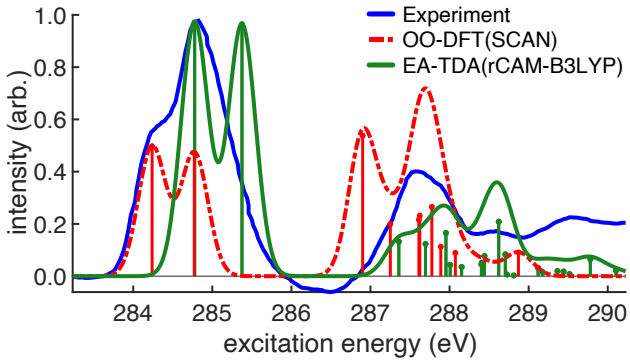

Figure S4: *trans*-butadiene K-edge X-ray absorption spectra for EA-TDA and OO-DFT juxtaposed against experimental data from Ref. 28. The third major peak (intensity of 0.6) in the OO-DFT spectrum corresponds to an optically dark 1s→3s transition and is absent in the EA-TDA spectrum. The aug-pcX-2 and aug-pcseg-1 basis sets were used for C and H, respectively.

References

[1] Epifanovsky, E. *et al.* Software for the frontiers of quantum chemistry: An overview of developments in the Q-Chem 5 package. *J. Chem. Phys.* **2021,** *155,* 084801:1–59.

[2] Verma, P.; Derricotte, W. D.; Evangelista, F. A. Predicting near edge x-ray absorption spectra with the spin-free exact-two-component Hamiltonian and orthogonality constrained density functional theory. *J. Chem. Theory Comput.* **2016,** *12,* 144–156.

[3] Dyall, K. G. Interfacing relativistic and nonrelativistic methods. I. Normalized elimination of the small component in the modified Dirac equation. *J. Chem. Phys.* **1997,** *106,* 9618–9626.

[4] Kutzelnigg, W.; Liu, W. Quasirelativistic theory equivalent to fully relativistic theory. *J. Chem. Phys.* **2005,** *123,* 241102.

[5] Iliaš, M.; Saue, T. An infinite-order two-component relativistic Hamiltonian by a simple one-step transformation. *J. Chem. Phys.* **2007,** *126,* 064102.

[6] Liu, W.; Peng, D. Exact two-component Hamiltonians revisited. *J. Chem. Phys.* **2009,** *131,* 031104.

[7] Saue, T. Relativistic Hamiltonians for Chemistry: A Primer. *ChemPhysChem* **2011,** *12,* 3077–3094.

[8] Li, Z.; Xiao, Y.; Liu, W. On the spin separation of algebraic two-component relativistic Hamiltonians. *J. Chem. Phys.* **2012,** *137,* 154114.

[9] Cheng, L.; Gauss, J. Analytic energy gradients for the spin-free exact two-component theory using an exact block diagonalization for the one-electron Dirac Hamiltonian. *J. Chem. Phys.* **2011,** *135,* 084114.

[10] Cunha, L. A.; Hait, D.; Kang, R.; Head-Gordon, M. Relativistic orbital-optimized density functional theory for accurate core-level spectroscopy. *J. Phys. Chem. Lett.* **2022,** *13,* 3438–3449.

[11] Gilbert, A. T. B.; Besley, N. A.; Gill, P. M. W. Self-consistent field calculations of excited states using the maximum overlap method (MOM). *J. Phys. Chem. A* **2008,** *112,* 13164–13171.

[12] Barca, G. M. J.; Gilbert, A. T. B.; Gill, P. M. W. Simple models for difficult electronic excitations. *J. Chem. Theory Comput.* **2018,** *14,* 1501–1509.

[13] Hait, D.; Head-Gordon, M. Excited state orbital optimization via minimizing the square of the gradient: General approach and application to singly and doubly excited states via density functional theory. *J. Chem. Theory Comput.* **2020,** *16,* 1699–1710.

[14] Carter-Fenk, K.; Herbert, J. M. State-targeted energy projection: A simple and robust approach to orbital relaxation of non-Aufbau self-consistent field solutions. *J. Chem. Theory Comput.* **2020,** *16,* 5067–5082.

[15] Worster, S. B.; Feighan, O.; Manby, F. R. Reliable transition properties from excited-state mean-field calculations. *J. Chem. Phys.* **2021,** *154,* 124106:1–9.

[16] Schirmer, J.; Trofimov, A. B.; Randall, K. J.; Feldhaus, J.; Bradshaw, A. M.; Ma, Y.; Chen, C. T.; Sette, F. K-shell excitation of the water, ammonia, and methane molecules using high-resolution photoabsorption spectroscopy. *Phys. Rev. A* **1993,** *47,* 1136–1147.

[17] Kramida, A.; Martin, W. C. A compilation of energy levels and wavelengths for the spectrum of neutral beryllium (Be I). *J. Phys. Chem. Ref. Data* **1997,** *26,* 1185–1194.

[18] Hitchcock, A. P.; Brion, C. E. Carbon K-shell excitation of C2H2, C2H4, C2H6 and C6H6 by 2.5 keV electron impact. *J. Electron Spectrosc. Relat. Phenom.* **1977,** *10,* 317–330.

[19] Remmers, G.; Domke, M.; Puschmann, A.; Mandel, T.; Xue, C.; Kaindl, G.; Hudson, E.; Shirley, D. A. High-resolution K-shell photoabsorption in formaldehyde. *Phys. Rev. A* **1992,** *46,* 3935–3944.

[20] Robin, M.; Ishii, I.; McLaren, R.; Hitchcock, A. Fluorination effects on the inner-shell spectra of unsaturated molecules. *J. Electron Spectrosc. Relat. Phenom.* **1988,** *47,* 53–92.

[21] Prince, K. C.; Richter, R.; de Simone, M.; Alagia, M.; Coreno, M. Near Edge X-ray Absorption Spectra of Some Small Polyatomic Molecules. *J. Phys. Chem. A* **2003,** *107,* 1955–1963.

[22] Hitchcock, A.; Brion, C. Inner shell electron energy loss studies of HCN and C2N2. *Chem. Phys.* **1979,** *37,* 319–331.

[23] Sodhi, R. N.; Brion, C. Reference energies for inner shell electron energy-loss spectroscopy. *J. Electron Spectrosc. Relat. Phenom.* **1984,** *34,* 363–372.

[24] Hitchcock, A.; Brion, C. K-shell excitation spectra of CO, N2 and O2. *J. Electron Spectrosc. Relat. Phenom.* **1980,** *18,* 1–21.

[25] Tronc, M.; King, G. C.; Read, F. H. Carbon K-shell excitation in small molecules by high-resolution electron impact. *J. Phys. B: At. Mol. Phys.* **1979,** *12,* 137–157.

[26] Prince, K. C.; Avaldi, L.; Coreno, M.; Camilloni, R.; Simone, M. d. Vibrational structure of core to Rydberg state excitations of carbon dioxide and dinitrogen oxide. *J. Phys. B: At. Mol. Opt. Phys.* **1999,** *32,* 2551–2567.

[27] Hempelmann, A.; Piancastelli, M. N.; Heiser, F.; Gessner, O.; Rüdel, A.; Becker, U. Resonant photofragmentation of methanol at the carbon and oxygen K-edge by high-resolution ion-yield spectroscopy. *J. Phys. B: At. Mol. Opt. Phys.* **1999,** *32,* 2677–2689.

[28] Sodhi, R.; Brion, C. High resolution carbon 1s and valence shell electronic excitation spectra of trans-1,3-butadiene and allene studied by electron energy loss spectroscopy. *J. Electron Spectrosc. Relat. Phenom.* **1985,** *37,* 1–21.

[29] Duflot, D.; Flament, J.-P.; Giuliani, A.; Heinesch, J.; Hubin-Franskin, M.-J. Core shell excitation of furan at the O1s and C1s edges: An experimental and ab initio study. *J. Chem. Phys.* **2003,** *119,* 8946–8955.

[30] Plekan, O.; Feyer, V.; Richter, R.; Coreno, M.; de Simone, M.; Prince, K.; Carravetta, V. An X-ray absorption study of glycine, methionine and proline. *J. Electron Spectrosc. Relat. Phenom.* **2007,** *155,* 47–53.

[31] Apen, E.; Hitchcock, A. P.; Gland, J. L. Experimental studies of the core excitation of imidazole, 4,5-dicyanoimidazole, and s-triazine. *J. Phys. Chem.* **1993,** *97,* 6859–6866.

[32] Pavlychev, A.; Hallmeier, K.; Hennig, C.; Hennig, L.; Szargan, R. Nitrogen K-shell excitations in complex molecules and polypyrrole. *Chem. Phys.* **1995,** *201,* 547–555.

[33] Okada, K.; Yoshida, H.; Senba, Y.; Kamimori, K.; Tamenori, Y.; Ohashi, H.; Ueda, K.; Ibuki, T. Angle-resolved ion-yield measurements of CO_2 in the O 1s to Rydberg excitation region. *Phys. Rev. A* **2002,** *66,* 032503.

[34] Hitchcock, A. P.; Brion, C. E. K-shell excitation of HF and F $_2$ studied by electron energy-loss spectroscopy. *J. Phys. B: At. Mol. Phys.* **1981,** *14,* 4399–4413.

[35] Hitchcock, A. P.; Brion, C. E. Neon K-shell excitation studied by electron energy-loss spectroscopy. *J. Phys. B: At. Mol. Phys.* **1980,** *13,* 3269–3273.

[36] Bodeur, S.; Millié, P.; Nenner, I. Single- and multiple-electron effects in the Si 1 *s* photoabsorption spectra of Si X 4 (X=H,D,F,Cl,Br, Ch 3 , C 2 H 5 , OCH 3 , OC 2 H 5) molecules: Experiment and theory. *Phys. Rev. A* **1990,** *41,* 252–263.

[37] Cavell, R. G.; Jürgensen, A. Chemical shifts in P-1s photoabsorption spectra of gaseous phosphorus compounds. *J. Electron Spectrosc. Relat. Phenom.* **1999,** *101-103,* 125–129.

[38] Reynaud, C.; Gaveau, M.-A.; Bisson, K.; Millié, P.; Nenner, I.; Bodeur, S.; Archirel, P.; Lévy, B. Double-core ionization and excitation above the sulphur K-edge in , and. *J. Phys. B: At. Mol. Opt. Phys.* **1996,** *29,* 5403–5419.

[39] Perera, R. C. C.; LaVilla, R. E. Molecular x-ray spectra: S- $K\ \beta$ emission and K absorption spectra of SCO and CS $_2$. *J. Chem. Phys.* **1984,** *81,* 3375–3382.

[40] Bodeur, S.; Hitchcock, A. Inner- and valence-shell excitation of SF4 studied by photoabsorption and electron energy loss spectroscopy. *Chem. Phys.* **1987,** *111,* 467–479.

[41] Reynaud, C.; Bodeur, S.; Maréchal, J. L.; Bazin, D.; Millié, P.; Nenner, I.; Rockland, U.; Baumgärtel, H. Electronic properties of the SF5Cl molecule: a comparison with SF6. I. Photoabsorption spectra near the sulphur K and chlorine K edges. *Chem. Phys.* **1992,** *166,* 411–424.

[42] Bodeur, S.; Maréchal, J. L.; Reynaud, C.; Bazin, D.; Nenner, I. Chlorine K shell photoabsorption spectra of gas phase HCl and Cl2 molecules. *Z. Phys. D* **1990,** *17,* 291–298.

[43] Lindle, D. W.; Cowan, P. L.; Jach, T.; LaVilla, R. E.; Deslattes, R. D.; Perera, R. C. C. Polarized x-ray emission studies of methyl chloride and the chlorofluoromethanes. *Phys. Rev. A* **1991,** *43,* 2353–2366.